Atmospheric
Chemistry
and Physics

Arctic spring and summertime aerosol optical depth baseline from long-term observations and model reanalyses – Part 1: Climatology and trend

Peng Xian[1], Jianglong Zhang[2], Norm T. O'Neill[3], Travis D. Toth[4], Blake Sorenson[2], Peter R. Colarco[5], Zak Kipling[6], Edward J. Hyer[1], James R. Campbell[1], Jeffrey S. Reid[1], and Keyvan Ranjbar[3,a]

[1]Naval Research Laboratory, Monterey, CA, USA
[2]Department of Atmospheric Sciences, University of North Dakota, Grand Forks, ND, USA
[3]Département de géomatique appliqué, Université de Sherbrooke, Sherbrooke, Quebec, Canada
[4]NASA Langley Research Center, Hampton, Virginia, USA
[5]NASA Goddard Space Flight Center, Greenbelt, MD, USA
[6]European Centre for Medium-Range Weather Forecasts, Reading, UK
[a]now at: Flight Research Laboratory, National Research Council Canada, Ottawa, ON, Canada

Correspondence: Peng Xian (peng.xian@nrlmry.navy.mil)

Abstract. We present an Arctic aerosol optical depth (AOD) climatology and trend analysis for 2003–2019 spring and summertime periods derived from a combination of multi-agency aerosol reanalyses, remote-sensing retrievals, and ground observations. This includes the U.S. Navy Aerosol Analysis and Prediction System Re-Analysis version 1 (NAAPS-RA v1), the NASA Modern-Era Retrospective Analysis for Research and Applications, version 2 (MERRA-2), and the Copernicus Atmosphere Monitoring Service ReAnalysis (CAMSRA). Spaceborne remote-sensing retrievals of AOD are considered from the Moderate Resolution Imaging Spectroradiometer (MODIS), the Multi-angle Imaging SpectroRadiometer (MISR), and the Cloud-Aerosol Lidar with Orthogonal Polarization (CALIOP). Ground-based data include sun photometer data from AErosol RObotic NETwork (AERONET) sites and oceanic Maritime Aerosol Network (MAN) measurements. Aerosol reanalysis AODs and spaceborne retrievals show consistent climatological spatial patterns and trends for both spring and summer seasons over the lower Arctic (60–70° N). Consistent AOD trends are also found for the high Arctic (north of 70° N) from reanalyses. The aerosol reanalyses yield more consistent AOD results than climate models, can be verified well with AERONET, and corroborate complementary climatological and trend analysis. Speciated AODs are more variable than total AOD among the three reanalyses and a little more so for March–May (MAM) than for June–August (JJA). Black carbon (BC) AOD in the Arctic comes predominantly from biomass burning (BB) sources in both MAM and JJA, and BB overwhelms anthropogenic sources in JJA for the study period.

AOD exhibits a multi-year negative MAM trend and a positive JJA trend in the Arctic during 2003–2019, due to an overall decrease in sulfate/anthropogenic pollution and a significant JJA increase in BB smoke. Interannual Arctic AOD variability is significantly large, driven by fine-mode and, specifically, BB smoke, with both smoke contribution and interannual variation larger in JJA than in MAM. It is recommended that climate models should account for BB emissions and BB interannual variabilities and trends in Arctic climate change studies.

1 Introduction

The Arctic is warming faster than the overall global climate, a phenomenon widely known as Arctic amplification (Serreze and Francis, 2006; Serreze and Barry, 2011). This has led to rapid changes in regional sea ice properties. September sea ice coverage is shrinking at an unprecedented rate (Comiso, 2012; Meier et al., 2014). Younger and thinner ice is replacing thick multi-year sea ice (Kwok and Rothrock, 2009; Hansen et al., 2013; Rosel et al., 2018). Mechanisms contributing to sea ice changes include increased anthropogenic greenhouse gases (Notz and Stroeve, 2016; Dai et al., 2019), sea-ice–albedo feedback (Perovich and Polashenski, 2012), increased warm and moist air intrusion into the Arctic (Boisvert et al., 2016; Woods and Caballero, 2016; Graham et al., 2017), radiative feedbacks associated with cloudiness and humidity (Kapsch et al., 2013; Morrison et al., 2018), and increased ocean heat transport (Nummelin et al., 2017; Taylor et al., 2018). However, one of the least understood factors of Arctic change is the impact of aerosols on sea ice albedo and concentration (IPCC, 2021a).

Atmospheric aerosol particles from anthropogenic and natural sources reach or can be found in the Arctic region as the result of long-range transport and local emissions, respectively. This affects regional energy balance through both direct and indirect radiative processes (Quinn et al., 2008; Engvall et al., 2009; Flanner, 2013; Sand et al., 2013; Markowicz et al., 2021; Yang et al., 2018). Aerosol particles influence cloud microphysical properties as cloud condensation nuclei (CCN) and/or ice-nucleating particles (INPs), affecting cloud albedo, lifetime, phase, and probability of precipitation (e.g., Lubin and Vogelmann, 2006; Lance et al., 2011; Zamora et al., 2016; Zhao and Garrett, 2015; Bossioli et al., 2021). Additionally, deposition of light-absorbing aerosol species such as dust and black/brown carbon on the surface of snow and ice can trigger albedo feedbacks and facilitate melting and prolong melting seasons (Hansen and Nazarenko, 2004; Jacobson, 2004; Flanner et al., 2007; Skiles et al., 2018; Dang et al., 2017; Kang et al., 2020). However, the impact of aerosol particles on polar climate change is still not well characterized, and their relative importance compared to other warming factors is difficult to isolate and quantify.

Climate modeling studies show that due to stronger feedback processes between the atmosphere–ocean–sea-ice–land, the Arctic region is more sensitive to local changes in radiative forcing than tropical and midlatitude regions (Shindell and Faluvegi, 2009; Sand et al., 2013). Furthermore, there seems to be an emerging agreement on a higher sensitivity of Arctic clouds by aerosol particles than lower-latitude regions due to the very low aerosol amounts compared to lower latitudes (Prenni et al., 2007; Mauritsen et al., 2011; Birch et al., 2012; Coopman et al., 2018; Wex et al., 2019). Both underscore the important role aerosol particles may play in the Arctic weather and climate and the urgency to better quantify the amount of aerosols in the Arctic.

A variety of atmospheric aerosol species exist in the Arctic region. Anthropogenic pollution contributes significantly to the formation of the Arctic haze, which generally occurs in later winter and spring due to wintertime build-up in the shallow boundary layer with effective transport and reduced removal (e.g., Law and Stohl, 2007; Quinn et al., 2008). Biomass burning (BB) smoke, originating from wildfires in boreal North America and Eurasia, is often observed and/or modeled being transported into the Arctic (Eck et al., 2009; Eckhardt et al., 2015; Stohl et al., 2007; Warneke et al., 2010; Iziomon et al., 2006; Evangeliou et al., 2016; Kondo et al., 2011; Breider et al., 2014; Markowicz et al., 2016; Khan et al., 2017; Engelmann et al., 2021). Airborne dust, emitted from exposed sand or soils due to glacier retreat (Bullard et al., 2016; Groot Zwaaftink et al., 2016), is likely on the rise as the Arctic warms. Dust can also originate from lower-latitude deserts, e.g., the Sahara and Asia, and arrive in the Arctic through long-range transport (Stone et al., 2007; Breider et al., 2014; AboEl-Fetouh et al., 2020). As the Arctic sea ice melts and the ice-free surface increases, emissions of sea salt and biogenic aerosols (e.g., from dimethylsulfide; Dall'Osto et al., 2017; Gabric et al., 2018) are expected to increase. There are also ultrafine particles nucleated from gaseous precursors, though in small amounts (Baccarini et al., 2020; Abbatt et al., 2019).

Because of the harsh surface environment endemic to the Arctic, aerosol field measurements are limited in comparison with the midlatitude and tropical environments. Despite an increasing number of field campaigns carried out over the past 2 decades (e.g., review by Wendisch et al., 2019, and more recently the MOSAiC, https://mosaic-expedition.org, last access: 28 June 2022) and their usefulness in improving process-level understanding, field measurement periods tend to be short and limited to certain areas and thus are not necessarily representative spatially and temporally of the whole Arctic. There are many Arctic aerosol optical property studies that are based on long-term site measurements (e.g., Herber et al., 2002; Tomasi et al., 2007; Eck et al., 2009; Glantz et al., 2014; Ranjbar et al., 2019; AboEl-Fetouh et al., 2020). The number of sites is, however, limited and of irregular spacing (mostly located at the northern edge of North America, the Eurasian continent, and the Svalbard region).

Climate models that are not well constrained by observations exhibit large variations in basic aerosol optical properties: one finds, for example, an order of magnitude difference in simulated regional aerosol optical depth (AOD) and large differences in the simulated seasonal cycle of AOD over the Arctic (e.g., Glantz et al., 2014; Sand et al., 2017). Such results will not reduce the uncertainty in the radiative impact of aerosols through direct (including surface albedo effect) and indirect forcings in the Arctic climate. Impacts of aerosols and clouds, overall, constitute one of the largest sources of uncertainty in climate models (IPCC, 2021b). This is apparently exacerbated in a warming Arctic (Goosse et al., 2018). A modeling study by DeRepentigny et al. (2021) shows that

the inclusion of interannually varying BB emissions, compared with only climatological emissions, results in simulations of large Arctic climate variability and enhanced sea ice loss. This finding suggests the sensitivity of climate-relevant processes to aerosol interannual variability in the Arctic.

In this paper, we present an AOD climatology and trend analysis for the 2003–2019 Arctic spring and summertime, based on a combination of multi-national interagency aerosol reanalyses, satellite remote-sensing retrievals, and ground observations. We define the Arctic and the high Arctic as regions north of 60 and 70° N, respectively. The lower Arctic is defined as regions between 60–70° N. To reference lower-latitude source influences, the area of 50–90° N is included for context.

There are clear advantages to using aerosol reanalyses of chemical transport models in comparison with climate models for Arctic aerosol studies. Smoke emissions are frequently updated (hourly rather than monthly BB smoke emission sources for example), while satellite observations of both meteorological and aerosol data are also incorporated into those aerosol reanalyses through data assimilation. High-latitude fires are strongly influenced by weather patterns including large-scale transport patterns (e.g., Flannigan and Harrington, 1988; Skinner et al., 1999). Thus, BB smoke in particular, is more realistically accounted for in aerosol reanalyses.

To our knowledge, this is the first time aerosol reanalysis products are evaluated and compared over the Arctic. The goal of the study is to provide a baseline of AOD distribution, magnitude, speciation, and interannual variability over the Arctic during the sea ice melting season. Statistics of Arctic extreme AOD events are provided in a companion paper (Xian et al., 2022). The baseline can be used for evaluating aerosol models, calculating aerosol radiative forcing, and providing background information for field campaign data analysis and future field campaign planning in a larger climate context. This paper is organized as follows: Sects. 2 and 3 introduce the datasets and methods, respectively. Section 4 verifies the reanalyses. Results are reported in Sect. 5. Discussions and conclusions are provided in Sects. 6 and 7.

2 Data

A combination of aerosol reanalyses, satellite-based aerosol remote-sensing data, and ground-based aerosol measurements are used to describe source-dependent AOD and its trend over the Arctic during spring (i.e., March–May, MAM) and summertime (i.e., June–August, JJA). The aerosol reanalyses include the Navy Aerosol Analysis and Prediction System reanalysis (NAAPS-RA; Lynch et al., 2016) developed at the Naval Research Laboratory, the NASA Modern-Era Retrospective Analysis for Research and Applications, version 2 (MERRA-2; Randles et al., 2017), and the Copernicus Atmosphere Monitoring Service ReAnaly-

sis (CAMSRA; Inness et al., 2019) produced at ECMWF. The remote-sensing data include AOD retrievals from the Moderate Resolution Imaging Spectroradiometer (MODIS; Levy et al., 2013), the Multi-angle Imaging SpectroRadiometer (MISR; Kahn et al., 2010), and the Cloud-Aerosol Lidar with Orthogonal Polarization (CALIOP). Sun photometer data from AErosol RObotic NETwork sites and oceanic Maritime Aerosol Network measurements were employed as key validation components (AERONET: Holben et al., 1998; MAN: Smirnov et al., 2009). Overviews of remote-sensing techniques for Arctic aerosols can be found in Tomasi et al. (2015) and Kokhanovsky and Tomasi (2020). The analysis period is focused on 2003–2019, when all three aerosol reanalyses are available. A summary of the datasets is provided in Appendix A.

2.1 MODIS AOD

AOD data from MODIS on Terra and Aqua were based on Collection 6.1 Dark Target and Deep Blue retrievals (Levy et al., 2013). Additional quality control and some corrections were applied as described in Zhang and Reid (2006), Hyer et al. (2011), and Shi et al. (2011, 2013) and were updated for the Collection 6.1 inputs. The 550 nm quality-assured and quality-controlled MODIS C6 AOD data are a level 3 product that is produced at $1° \times 1°$ latitude–longitude spatial and 6-hourly temporal resolution. Those 6-hourly (averaged) MODIS AOD data were then monthly binned in order to study long-term aerosol climatology and trends. Seasonally binned (year-to-year) means and trends were derived only when the total count of $1° \times 1°$ and 6-hourly data exceeded 10 for a season.

2.2 MISR AOD

The MISR instrument onboard the Terra satellite platform provides observations at nine different viewing zenith angles across four different spectral bands ranging from 446 to 866 nm. These instrumental configurations facilitate AOD retrievals over bright surfaces, such as desert regions (Kahn et al., 2010). MISR Version 23 AOD data at 558 nm (Garay et al., 2020) were analyzed. No MISR AOD is available over Greenland due to snow and ice coverage. Monthly gridded MISR AOD data were created by averaging only MISR data with 100 % clear pixels (as defined by each pixel's "cloud screening parameter") at a spatial resolution of $1° \times 1°$ latitude–longitude. Only monthly grid cells whose number of MISR 100 %-cloud-clear AODs was greater than 20 were used to derive the climatology and trend.

2.3 CALIOP AOD

The Cloud-Aerosol Lidar with Orthogonal Polarization (CALIOP), the primary instrument on the Cloud-Aerosol Lidar and Infrared Pathfinder Satellite Observations

(CALIPSO) satellite, is a polarization-sensitive lidar that operates at two wavelengths (532 and 1064 nm; Winker et al., 2003). It has, since its launch in 2006, collected a continuity of vertical aerosol and cloud profiles. We primarily used daytime and nighttime 532 nm aerosol extinction coefficient data from the Version 4.2 (V4.2) Level 2 (L2) aerosol profile product (Kim et al., 2018). The product resolution is 5 km in the horizontal and 60 m in the vertical. The aerosol layer product was used for quality assurance (QA) procedures. The CALIOP aerosol profiles are rigorously quality-assured before analysis (Campbell et al., 2012; Toth et al., 2016, 2018). Only cloud-free CALIOP profiles are used: this was determined through the atmospheric volume description (AVD) parameter included in the aerosol profile product (i.e., we excluded CALIOP profiles with any range bin classified as cloud by the AVD parameter). A significant portion of CALIOP aerosol profile data consists of retrieval fill values (−9999 or RFVs) that are, in part, due to the minimum detection limits of the lidar. In fact, over 80 % of CALIOP profiles consist entirely of RFVs in some Arctic regions (Toth et al., 2018). These result in zero-valued column AODs: their inclusion in composites would artificially lower the mean AOD. They were thus excluded from our analysis. We also tested retaining AOD $= 0$ values in our analysis and that did not change the AOD trends (see more discussions in Sect. 6). Lastly, the cloud-free quality-assured profiles without AOD $= 0$ profiles were used to compute mean CALIOP AODs at a $2° \times 5°$ latitude–longitude resolution. To ensure spatial and temporal representation, seasonally binned means and trends were derived only when the total count of gridded data in any season exceeded 20.

2.4 AERONET

The AErosol RObotic NETwork (AERONET) is a ground-based global sun photometer network. AERONET instruments measure sun and sky radiance in spectral bands ranging from the near-ultraviolet to the short-wave infrared. This network has been providing daytime aerosol-property measurements since the 1990s (Holben et al., 1998, 2001). Only cloud-screened, quality-assured version 3 Level 2 AERONET data (Giles et al., 2019) are used in this study.

The 500 nm fine-mode (FM) and coarse-mode (CM) AODs from the spectral deconvolution algorithm (SDA) of O'Neill et al. (2001, 2003), along with the FM spectral derivative at 500 nm, are used to extrapolate FM AOD to 550 nm (assuming equal CM AOD at 500 and 550 nm). Total AOD is simply the sum of FM and CM AODs. The SDA product is an AERONET product that has been verified using in situ measurements (see for example Kaku et al., 2014) and a variety of co-located lidar experiments (see, for example, Saha et al., 2010, and Baibakov et al., 2015). The FM and CM separation is effected spectrally: this amounts to a separation of the FM and CM optical properties associated with their complete FM and CM particle size distributions. This

optical separation, characterized by the ratio of FM AOD to total AOD at 550 nm is referred to as the fine-mode fraction (FMF). An analogous FM and CM AOD separation in terms of a cutoff radius applied to a retrieved or measured particle size distribution is referred to as the sub-micron fraction (SMF; where the numerator of the SMF is the FM AOD associated with the AOD contribution of particles below a cutoff radius). The SMF is the basis for separating FM and CM components in the AERONET (AOD and sky radiance) inversion. The SDA algorithm and the AERONET inversion generate FM and CM AODs that are moderately different (see, for example, Sect. 4 of Kleidman et al., 2005). The advantage of the SDA is its significantly shorter intersampling time and thus retrieval numbers ($\sim 20\,h^{-1}$ vs. $\sim 1\,h^{-1}$ for the AERONET inversion), its independence from a variable cutoff radius, and its greater operational generality (being applicable to other networks such as the MAN sun photometer network).

AERONET data were binned into 6 h intervals centered at normal synoptic output times of the reanalyses (00:00, 06:00, 12:00, and 18:00 UTC) and then averaged within the bins. Monthly mean temporal representativeness was rendered more likely by only including means with more than eighteen 6 h data bins. Ten AERONET sites (Table 1, Fig. 1) were selected based on regional representativeness (coupled with the reality of the sparsity of AERONET sites in the Arctic) and the availability of data records between January 2003 and December 2019, and for easier comparison with other Arctic studies (e.g., Sand et al., 2017). To explore the potential impact of different sampling resolutions on the results (e.g., Balmes et al., 2021), we generated daily AOD statistics (Table S1) that could be compared with Table 1 6-hourly statistics. In general, the mean and median of MAM or JJA AODs (including total, FM, and CM AODs) at the 10 AERONET sites change very slightly (mostly 0.00, or ≤ 0.01). The daily AOD standard deviation was less than its 6-hourly analogue.

We found that thin clouds could occasionally be identified and retrieved as CM aerosols in level 2, version 3 AERONET data. These retrievals were manually removed by identifying such thin clouds using Terra and Aqua visible-wavelength imagery from NASA Worldview and comparing 6-hourly NAAPS-RA with AERONET AODs. CM AODs greater than the 3σ level were then also removed (as per AboEl-Fetouh et al., 2020).

2.5 MAN AOD

The Marine Aerosol Network (MAN) is a handheld Microtops sun photometer (research-vessel-based) counterpart to AERONET: ocean measurements are acquired where no land-based AERONET site can exist (Smirnov et al., 2009, 2011). The products share AERONET product nomenclature, and data processing is similar to that of AERONET. Level 2 data above 70° N were employed in this study. SDA-

Table 1. Geographical coordinates of AERONET sites used in this study and seasonally binned mean, median, and standard deviation of the total AOD and SDA-derived FM and CM AOD at 550 nm for MAM and JJA based on 2003–2019 data when available. The last row shows the same statistics for MAN AODs acquired north of 70° N. "n" represents the number of 6-hourly AERONET or MAN data.

Sites	Latitude	Longitude	Elev. (m)	Region	MAM (mean | median | SD) total AOD			FM AOD			CM AOD			n	MAM FMF mean	median	JJA (mean | median | SD) total AOD			FM AOD			CM AOD			n	JJA FMF mean	median
Hornsund	77.0° N	15.6° E	12	Svalbard	0.10	0.09	0.05	0.07	0.06	0.04	0.03	0.02	0.03	846	0.71	0.75	0.08	0.06	0.07	0.06	0.04	0.07	0.02	0.01	0.01	971	0.77	0.83
Thule	76.5° N	68.8° W	225	Greenland	0.08	0.07	0.05	0.06	0.05	0.03	0.03	0.01	0.04	1009	0.75	0.81	0.07	0.05	0.06	0.06	0.04	0.06	0.01	0.01	0.02	1509	0.85	0.88
Kangerlussuaq	67.0° N	50.6° W	320	Greenland	0.07	0.06	0.04	0.05	0.04	0.02	0.02	0.02	0.03	957	0.69	0.72	0.07	0.05	0.05	0.05	0.04	0.05	0.01	0.01	0.01	1768	0.77	0.78
Ittoqqortoormiit	70.5° N	21.0° W	68	Greenland	0.06	0.05	0.04	0.04	0.04	0.02	0.02	0.01	0.03	545	0.72	0.78	0.06	0.04	0.04	0.05	0.03	0.05	0.01	0.01	0.02	1280	0.80	0.81
Andenes	69.3° N	16.0° E	379	Norway	0.08	0.07	0.05	0.05	0.04	0.03	0.03	0.02	0.03	821	0.67	0.71	0.08	0.07	0.05	0.06	0.05	0.05	0.02	0.01	0.02	1008	0.75	0.78
Resolute_Bay	74.7° N	94.9° W	35	Nunavut	0.10	0.08	0.05	0.07	0.06	0.03	0.03	0.02	0.03	520	0.73	0.78	0.08	0.05	0.10	0.06	0.04	0.10	0.02	0.01	0.03	1178	0.78	0.83
Barrow	71.3° N	156.7° W	8	Alaska	0.11	0.09	0.07	0.08	0.06	0.05	0.03	0.02	0.04	605	0.73	0.77	0.10	0.07	0.15	0.08	0.05	0.15	0.02	0.01	0.02	1155	0.79	0.82
Bonanza_Creek	64.7° N	148.3° W	353	Alaska	0.10	0.08	0.09	0.06	0.04	0.08	0.04	0.03	0.04	953	0.61	0.60	0.21	0.09	0.36	0.18	0.06	0.35	0.03	0.02	0.03	1717	0.75	0.76
Tiksi	71.6° N	129.0° E	17	Siberia	0.10	0.10	0.03	0.08	0.08	0.03	0.02	0.01	0.02	39	0.80	0.82	0.13	0.08	0.18	0.11	0.07	0.17	0.02	0.01	0.02	449	0.80	0.85
Yakutsk	61.7° N	129.4° E	119	Siberia	0.15	0.11	0.15	0.11	0.08	0.13	0.04	0.02	0.04	1516	0.76	0.80	0.16	0.09	0.24	0.14	0.07	0.24	0.02	0.01	0.02	2579	0.81	0.84
MAN	>70° N	–		Arctic Ocean	0.11	0.10	0.06	0.06	0.06	0.04	0.04	0.04	0.03	85	0.62	0.62	0.06	0.05	0.07	0.04	0.03	0.07	0.02	0.02	0.01	435	0.66	0.67

based FM and CM AOD at 550 nm were derived and averaged over 6 h time bins.

2.6 NAAPS AOD reanalysis v1

The Navy Aerosol Analysis and Prediction System (NAAPS) AOD ReAnalysis (NAAPS-RA) v1 provides 550 nm, global-scale, speciated AODs at $1° \times 1°$ spatial and 6-hourly temporal resolution for the years 2003–2019 (Lynch et al., 2016). This NAAPS-based reanalysis incorporates the assimilation of quality-controlled MODIS and MISR AOD retrievals (Zhang and Reid, 2006; Hyer et al., 2011; Shi et al., 2011). AODs from anthropogenic and biogenic fine aerosol species (ABF; a non-BB sources mixture of sulfate, black carbon, organic aerosols, and secondary organic aerosols), dust, BB smoke, and sea salt aerosols are available. The aerosol source functions were tuned to obtain the best match between the model FM and CM AODs and the AERONET AODs for 16 regions globally. Wet-deposition processes were constrained with satellite-derived precipitation (Xian et al., 2009). The reanalysis reproduces the decadal AOD trends found using standalone satellite products (e.g., Zhang and Reid, 2010; Zhang et al., 2017, who excluded polar regions due to lack of verification data).

2.7 MERRA-2 AOD reanalysis

NASA Modern-Era Retrospective Analysis for Research and Applications, version 2 (MERRA-2), includes an aerosol reanalysis scheme that incorporates AOD assimilation of a variety of remote-sensing data sources, including MODIS and MISR after 2000. The aerosol module used for MERRA-2 is the Goddard Chemistry, Aerosol Radiation and Transport model (GOCART; Chin et al., 2000; Colarco et al., 2010). It provides simulations of sulfate, black and organic carbon, dust, and sea salt aerosols. A detailed description and global validation of the AOD reanalysis product can be found in Randles et al. (2017) and Buchard et al. (2017). Monthly mean speciated AODs and total AOD at 550 nm with 0.5° latitude and 0.625° longitude spatial resolution were used for this study.

2.8 CAMSRA AOD reanalysis

The Copernicus Atmosphere Monitoring Service (CAMS) Reanalysis (CAMSRA) is a new ECMWF-led global reanalysis of atmospheric composition (Inness et al., 2019). It followed on the heels of the MACC reanalysis (Inness et al., 2013) and CAMS interim reanalysis (Flemming et al., 2017). The dataset covers the period of 2003–2020 and is being extended to subsequent years. The model is driven by the Integrated Forecasting System (IFS) used at ECMWF for weather forecasting and meteorological reanalysis (but at a coarser resolution). It incorporates additional modules activated for prognostic trace gases and aerosol species, includ-

ing dust, sea salt, organic matter, black carbon, and sulfate. Satellite retrievals of total AOD at 550 nm are assimilated from MODIS for the whole period and from the Advanced Along-Track Scanning Radiometer for 2003–2012, using a 4D variational data assimilation system with a 12 h data assimilation window along with meteorological and trace gas observations. The speciated AOD products with monthly temporal resolution and a $\sim 0.7°$ spatial resolution were used in this study. Model development has generally improved the speciation of aerosols compared with earlier reanalyses, and evaluation against AERONET globally is largely consistent over the period of the reanalysis.

2.9 Multi-reanalysis consensus (MRC) AOD

All three of the individual reanalyses are largely independent in their underlying meteorology and in their aerosol sources, sinks, microphysics, and chemistry. They were also generated through data assimilation of satellite and/or ground-based observations of AOD. The assimilation methods and the assimilated AOD observations, including the treatments of the observations prior to assimilation (quality control, bias correction, aggregation, and sampling, etc.), often differ. There is, on the other hand, consistent use of MODIS data with its daily global spatial coverage.

Based on the three aerosol reanalysis products described above, we made an MRC product following the multi-model-ensemble method of the International Cooperative for Aerosol Prediction (ICAP, Sessions et al., 2015; Xian et al., 2019). The MRC is a consensus mean of the three individual reanalyses, with a $1° \times 1°$ spatial and monthly temporal resolution. Speciated AODs and total AOD at 550 nm for 2003–2019 are available. This new product is validated here, along with the three component reanalysis members, using ground-based Arctic AERONET observations. Validation results in terms of bias, RMSE, and coefficient of determination (r^2) for monthly mean total, FM, and CM AODs are presented in Tables 2–4. The MRC, in accordance with the ICAP multi-model consensus evaluation result, is found to generally be the top performer among all of the reanalyses for the study region.

2.10 Fire Locating and Modeling of Burning Emissions (FLAMBE) v1.0

FLAMBE is a biomass burning emission inventory derived from a satellite-based active fire hotspot approach (Reid et al., 2009; Hyer et al., 2013). FLAMBE can take satellite fire products from either geostationary sensors, which offer faster refresh rates and observation of the full diurnal cycle, or polar orbiters, which have a greater sensitivity. There are significant daily sampling biases and additional artifacts induced by day-to-day shifts in the orbital pattern for polar-orbiting satellites (e.g., Heald et al., 2003; Hyer et al., 2013). However, the polar-only version of FLAMBE, which em-

Table 2. Total, FM, and CM AOD bias of CAMSRA, MERRA-2, NAAPS-RA, and their consensus mean MRC compared to AERONET monthly data.

Sites	Bias total AOD				Bias FM AOD				Bias CM AOD			
	CAMSRA	MERRA2	NAAPS-RA	MRC	CAMSRA	MERRA2	NAAPS-RA	MRC	CAMSRA	MERRA2	NAAPS-RA	MRC
Hornsund	−0.02	0.01	0.00	0.00	−0.01	0.01	−0.01	0.00	−0.01	0.01	−0.01	0.00
Thule	0.00	0.02	0.00	0.01	0.01	0.02	−0.01	0.01	0.01	0.00	−0.01	0.00
Kangerlussuaq	0.02	0.02	0.02	0.02	0.03	0.02	0.02	0.02	−0.01	0.00	−0.01	0.00
Ittoqqortoormiit	0.04	0.03	0.02	0.03	0.04	0.02	0.00	0.02	0.00	0.01	0.02	0.01
Andenes	0.03	0.04	0.02	0.03	0.03	0.02	0.00	0.02	0.00	0.02	0.01	0.01
Resolute_Bay	0.01	0.02	0.01	0.01	0.03	0.02	0.00	0.02	−0.02	0.00	0.00	0.00
Barrow	0.02	0.03	0.00	0.02	0.04	0.03	−0.01	0.02	−0.02	0.00	0.02	0.00
Bonanza_Creek	0.06	0.04	0.00	0.03	0.09	0.05	0.00	0.05	−0.02	−0.01	0.00	−0.01
Tiksi	0.02	0.02	−0.01	0.01	0.04	0.02	−0.01	0.02	−0.02	0.00	0.01	0.00
Yakutsk	0.03	0.04	0.01	0.03	0.05	0.05	0.00	0.03	−0.01	0.00	0.01	−0.01
Mean	0.02	0.03	0.01	0.02	0.04	0.03	0.00	0.02	−0.01	0.00	0.01	0.00
Median	0.02	0.03	0.01	0.02	0.04	0.02	0.00	0.02	−0.02	0.00	0.02	0.00

Table 3. Same as Table 2 except for RMSE.

Sites	RMSE total AOD				RMSE FM AOD				RMSE CM AOD			
	CAMSRA	MERRA2	NAAPS-RA	MRC	CAMSRA	MERRA2	NAAPS-RA	MRC	CAMSRA	MERRA2	NAAPS-RA	MRC
Hornsund	0.04	0.02	0.02	0.02	0.03	0.02	0.02	0.02	0.02	0.01	0.02	0.01
Thule	0.02	0.03	0.02	0.02	0.03	0.03	0.02	0.02	0.02	0.01	0.02	0.01
Kangerlussuaq	0.03	0.03	0.03	0.03	0.04	0.02	0.02	0.02	0.01	0.01	0.02	0.01
Ittoqqortoormiit	0.04	0.03	0.02	0.03	0.05	0.03	0.01	0.02	0.01	0.01	0.02	0.01
Andenes	0.03	0.04	0.03	0.03	0.03	0.03	0.02	0.02	0.01	0.02	0.03	0.02
Resolute_Bay	0.03	0.04	0.02	0.03	0.04	0.04	0.02	0.03	0.02	0.01	0.02	0.01
Barrow	0.05	0.05	0.03	0.04	0.06	0.04	0.03	0.03	0.02	0.01	0.02	0.01
Bonanza_Creek	0.11	0.10	0.07	0.08	0.12	0.10	0.06	0.08	0.03	0.02	0.01	0.02
Tiksi	0.05	0.04	0.02	0.03	0.06	0.04	0.02	0.03	0.02	0.01	0.01	0.01
Yakutsk	0.07	0.07	0.04	0.06	0.08	0.07	0.04	0.06	0.03	0.01	0.01	0.01
Mean	0.05	0.05	0.03	0.04	0.05	0.04	0.03	0.03	0.02	0.01	0.02	0.01
Median	0.04	0.04	0.03	0.03	0.05	0.04	0.02	0.03	0.02	0.01	0.02	0.01

Table 4. Same as Table 2 except for r^2.

Sites	r^2 total AOD				r^2 FM AOD				r^2 CM AOD			
	CAMSRA	MERRA2	NAAPS-RA	MRC	CAMSRA	MERRA2	NAAPS-RA	MRC	CAMSRA	MERRA2	NAAPS-RA	MRC
Hornsund	0.23	0.78	0.75	0.73	0.35	0.73	0.71	0.67	0.27	0.45	0.55	0.56
Thule	0.50	0.47	0.73	0.64	0.52	0.45	0.70	0.62	0.01	0.26	0.44	0.41
Kangerlussuaq	0.48	0.54	0.42	0.53	0.52	0.52	0.35	0.52	0.00	0.57	0.16	0.35
Ittoqqortoormiit	0.68	0.75	0.67	0.79	0.63	0.81	0.76	0.83	0.24	0.36	0.14	0.35
Andenes	0.67	0.63	0.68	0.71	0.68	0.66	0.64	0.71	0.10	0.23	0.21	0.21
Resolute_Bay	0.52	0.51	0.67	0.63	0.53	0.49	0.73	0.62	0.02	0.06	0.03	0.05
Barrow	0.33	0.68	0.70	0.62	0.45	0.76	0.69	0.68	0.05	0.27	0.41	0.41
Bonanza_Creek	0.81	0.78	0.80	0.83	0.83	0.79	0.82	0.85	0.06	0.43	0.45	0.46
Tiksi	0.77	0.80	0.87	0.84	0.82	0.82	0.90	0.86	0.02	0.20	0.10	0.15
Yakutsk	0.70	0.70	0.80	0.77	0.78	0.71	0.80	0.80	0.01	0.41	0.42	0.42
Mean	0.57	0.66	0.71	0.71	0.61	0.67	0.71	0.72	0.08	0.32	0.29	0.34
Median	0.60	0.69	0.72	0.72	0.58	0.72	0.72	0.70	0.04	0.32	0.31	0.38

ployed MODIS-based fire data, is more appropriate for re-analysis and trend analysis. This is because multiple changes in the geostationary constellation over the study period posed a challenge in terms of smoke source-function consistency. The FLAMBE MODIS-only smoke source was also used in the NAAPS-RA v1 because of the same temporal consistency requirement. FLAMBE shows similar BB emission trends as the yearly BB emission time series for the Arctic region based on other inventories for a similar study period (using the BC emission of Fig. 2 in McCarty et al., 2021). These inventories include the Global Fire Assimilation System (GFAS; Kaiser et al., 2012), and the Global Fire Emission Dataset (GFED; Randerson et al., 2006; van der Werf et al., 2006).

3　Method

The Arctic AOD climatology and trends are analyzed in this study using remote-sensing products derived from MODIS, MISR, CALIOP, and AERONET (each sensor typically generating aerosol products of different native wavelengths). The 550 nm AOD was employed as the benchmark parameter since the three aerosol reanalyses AODs and the MODIS AOD are all available at 550 nm, while the 558 and 532 nm AODs of MISR and CALIOP are appreciably close to 550 nm. AERONET and MAN modal AODs at 550 nm were derived using the SDA method as described in Sect. 2.4 and 2.5. Arithmetic means were employed for all the data processing in order to be consistent with the arithmetic statistics that are usually reported in the literature and with the arithmetic statistics of the monthly data from the aerosol reanalyses. Various studies have shown that geometric statistics are more representative of AOD histograms (see, for example, Hesaraki et al., 2017; Sayer and Knobelspiesse, 2019). However, Hesaraki et al. (2017) showed that arithmetic statistics could be employed to readily estimate geometric statistics.[1] This option effectively renders the reporting of arithmetic or geometric statistics less critical.

The species of interest are BB smoke, ABF in NAAPS, and its analogue of sulfate for MERRA-2 as well as CAMSRA, and dust and sea salt aerosols. Anthropogenic aerosol particles, as external climate forcers, have attracted some attention in climate studies (e.g., Wang et al., 2018; Ren et al., 2020; Yang et al., 2018; Sand et al., 2016; Eckhardt et al., 2015; Breider et al., 2017). However, BB smoke, which can be both natural and anthropogenic in origin, has been shown to be the largest contributor (over the last 2 decades) to Arctic summer AOD and concentration (Evangeliou et al., 2016, Sand et al., 2017, for modeling studies and Eck et al., 2009, Eckhardt et al., 2015, Stohl et al., 2007, Warneke et al., 2010, for observationally based studies). Recent BC measurements

---

[1]With an erratum: the Eq. (2) transformation to geometric mean should be $\tau_{g,x} = \frac{\langle \tau_x \rangle}{\exp\left(\frac{\ln^2 \mu_x}{2}\right)}$.

in Arctic snow also show a strong association with BB based on modeled tracer correlations with measured optical properties of snow (Hegg et al., 2009; Doherty et al., 2010; Hegg et al., 2010; Khan et al., 2017). A climate modeling study recently found that much larger Arctic climate variability and enhanced sea ice melting were introduced using BB emissions with interannual variability as opposed to fixed climatological monthly mean BB emissions (DeRepentigny et al., 2021), a result that underscored the importance of quantifying the magnitude and interannual variability of BB smoke in Arctic climate forcing estimates. Thus BB smoke AOD is separated out from the total AOD as a singularly important species in this study.

The separation of species in this analysis is a bit arbitrary since the representation of different aerosol types and sources in each reanalysis is slightly different. The NAAPS model is unique compared to other reanalyses and operational models in that it carries aerosol species by source rather than chemical speciation. For example, biomass burning and ABF are carried as separate species and permit explicit hypothesis testing about the sources, sinks, and optical properties. Conversely, MERRA-2 and CAMSRA carry organic carbon (OC) and organic matter (OM) respectively, BC, and various inorganic species combining a multitude of anthropogenic, biogenic, and biomass burning source pathways. In this study the sum of OC/OM and BC AOD is used to approximate BB smoke AOD from CAMSRA/MERRA-2. The ratio of BC AOD to the sum of BC and OC/OM AOD is, on average, about 10 % for areas north of 60° N for MERRA-2/CAMSRA for both MAM and JJA (the single exception to this is that the MERRA-2 ratio is about 18 % in MAM). The ratios change little for areas > 70° N and areas > 80° N.

It is worth noting that the three reanalyses use either hourly or daily BB smoke emission inventories: inventories that employ dynamic smoke sources detected by polar-orbiting satellites. Examples include FLAMBE (Reid et al., 2009) for NAAPS-RA, the Quick Fire Emissions Dataset (QFED) for MERRA-2 after 2010 (GFED with monthly BB emission before 2010 as per Randerson et al., 2006; van der Werf et al., 2006), and the Global Fire Assimilation System (GFAS, Kaiser et al., 2012) for CAMSRA. This is expected to yield a better spatial and temporal representation of BB smoke emissions compared to climate models which use monthly mean BB inventories (e.g., Sand et al., 2017).

We also assume all dust and sea salt are CM, while other model aerosol species, including ABF in NAAPS-RA, sulfate in MERRA-2 and CAMSRA, BB smoke in NAAPS-RA, and BC and OC/OM in MERRA-2/CAMSRA are FM aerosol particles. This approximation (the sequestering of dust and sea salt to the CM regime) is based on the fact that FM dust and sea salt only contribute a small portion of the total dust or sea salt AOD at 550 nm. For example, FM dust represents about 30 % and 39 % of total dust AOD globally in MERRA-2 and CAMSRA, respectively. The numbers are 17 % and 10 % for sea salt. NAAPS-RA makes the simpli-

fying microphysical assumption that all dust and sea salt are CM.

For verification purposes, the bias, root-mean-square error (RMSE) and coefficient of determination (denoted r^2) of reanalysis AODs compared to AERONET/MAN AODs are calculated. r^2 equals the square of the Pearson correlation coefficient between the observed and the modeled AODs. When estimating contributions of individual species to total-AOD interannual variability, r^2 is calculated as the square of the Pearson correlation coefficient between the seasonally binned modeled speciated AOD and total AOD. In that form, r^2 provides the percentage of "explained variance" of total AOD by a speciated AOD. The statistical definition and interpretation of r^2 can be found at https://en.wikipedia.org/wiki/Coefficient_of_determination (last access: 10 July 2022).

The significance test for trend analysis applies the same calculation method as in Zhang and Reid (2010), Zhang et al. (2017), an approach which, in turn, was based on the method of Weatherhead et al. (1998). This trend analysis method requires a continuous time series of data.

4 Comparison of AODs from aerosol reanalyses and AERONET

The number of AERONET observations are tied to the increase in the number of daylight hours and are therefore more numerous during the summer than in the spring. This translates to their generally being more temporally representative of 6 h or daily means in JJA. As a consequence, we preferentially used a JJA climatology to illustrate reanalyses vs. AERONET comparisons. Figure 1 shows the mean JJA FM and CM AODs from AERONET and the speciated AODs from NAAPS-RA, MERRA-2, and CAMSRA. All three aerosol reanalyses appear to capture the total-AOD magnitudes to varying extents. The AERONET retrievals show that total AOD during the Arctic JJA season is dominated by contributions from FM aerosols. Large FM AOD values (generally indicative of strong BB smoke influence) are found in Yakutsk and Tiksi in Siberia and Bonanza Creek in Alaska. CM aerosols also contribute a substantial fraction, varying from a minimum of 15 % in regions close to BB smoke sources to a maximum of $\sim 25\%$ at the Norwegian Sea and Greenland Sea coastal sites (Hornsund, Andenes, and Ittoqqortoormiit): these sites are likely impacted by sea salt aerosols lifted by North Atlantic cyclonic events. NAAPS-RA produces AERONET-comparable FM and total AODs in general while showing a tendency to overestimate CM AODs (see Table 2 for explicit biases). The other two reanalyses produce higher FM AOD and total AOD and lower CM AOD compared to AERONET (see also Table 2).

Differences exist between the three reanalyses with respect to the FM and CM partitioning of aerosol species. For example, sea salt aerosols always dominate in the CAMSRA (dust + sea salt) CM: this comment even applies to some in-

land sites (e.g., Bonanza Creek) and implies a modeling issue. Dust is the dominant CM species in NAAPS-RA and MERRA-2. This is true at all AERONET site positions: it is likely attributable to elevated dust layers transported from lower latitudes (Stone et al., 2007; Jacob et al., 2010; Breider et al., 2014; AboEl-Fetouh et al., 2020). The proportional contribution of dust to total AOD is at its largest in NAAPS-RA: a result that could have contributed to its high bias in CM AOD (Table 2). The contribution of organic matter to FM AOD is generally larger in CAMSRA than in the other two reanalyses. On the whole, BB smoke is the largest contributing species to total JJA AOD over the Arctic. This is consistent across all the reanalyses except for some sites in NAAPS-RA (e.g., Andenes, Hornsund, and Kangerlussuaq where ABF AOD is slightly larger than BB smoke AOD). This can be partially due to the different types of speciation employed in NAAPS-RA: ABF represents anthropogenic and biogenic pollution aerosols. The ABF category includes sulfate, BC, and (with the exception of BB aerosols) organic aerosols of all origins. It is also worth noting that mean AERONET AODs are, in general, higher (0.01–0.02 and can be ~ 0.1 higher for the sites close to BB sources) than their median counterparts (Table 1) as well as their geometric means. This is because AOD histograms are typically more lognormal than normal in form (asymmetric linear-AOD histograms with positively skewed tails as per, for example, Hesaraki et al., 2017): arithmetic means are, accordingly, often driven by extreme ($> 95\%$ percentile for example) AOD events. Because these extreme events constitute an important part of the Arctic aerosol environment, the AOD means are presented here.

The geographical coordinates of the 10 AERONET sites are provided in Table 1 as are the mean, median, and standard deviation of the total, FM, and CM AODs at 550 nm for both MAM and JJA based on available data (the availability of AERONET data can be seen in the monthly time series in Fig. 2). Analogous MAN statistics are provided in the last row of Table 1 (see also Fig. S1 for geographical distributions of MAN measurements). The seasonal mean total AOD for Resolute Bay, the Greenland sites, Hornsund and the MAN measurements is $\lesssim 0.1$ (0.06–0.10), while the Alaskan and Siberian site values are $\gtrsim 0.1$ (0.10 to 0.15, with Bonanza Creek displaying a substantially larger JJA value of 0.21). All sites, except Bonanza Creek, tend to have moderately higher median AOD in MAM: this is consistent with other Arctic sun photometer studies (Tomasi et al., 2015; Xie et al., 2018). The lower values in JJA, according to the reanalyses (Figs. 4 and 5), is related to higher FM ABF/sulfate and/or CM dust and sea salt in MAM. This AOD seasonal difference may have evolved in the past 2 decades with a decreasing trend in ABF/sulfate as discussed in Sect. 5.3. The mean AOD is greater in JJA than in MAM for Yakutsk, Tiksi, and Bonanza Creek: this is likely due to strong FM AOD variations associated with BB smoke events (see, for example, the discussions concerning the seasonal competition between FM
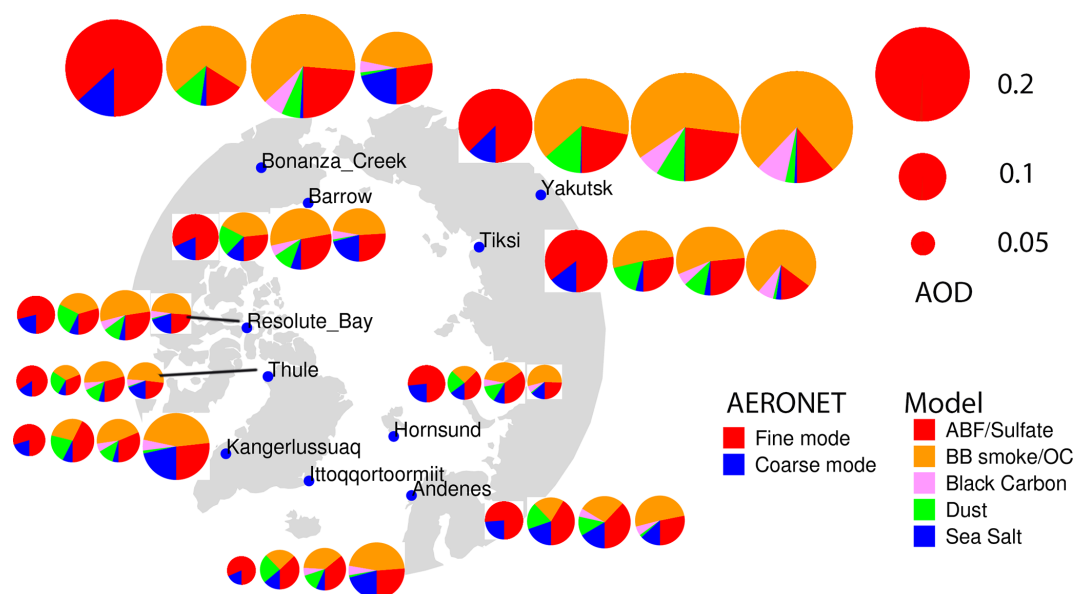
Figure 1. Polar projection map showing the locations of the AERONET Arctic sites (small solid blue circles) used in this study. Long-term (2003–2019) JJA-mean FM and CM AODs at 550 nm from AERONET (leftmost circle of each group of four circles) and, respectively, the speciated pie charts of 550 nm AODs from NAAPS-RA, MERRA-2, and CAMSRA for each site. Warm colors (red, orange, and pink) represent FM and cool colors (green and blue) represent CM. Circle size varies with AOD magnitude (see the key to the top right).

AOD smoke and FM AOD Arctic haze in AboEl-Fetouh et al., 2020). The standard deviations of the total and FM AODs are also high for those three sites.

The Table 1 median and mean of the FMF vary, respectively, between 0.60 to 0.88 and 0.61 to 0.85 with higher FMF in JJA than in MAM. The MAN measurements have higher CM AODs and lower FMF compared to AERONET measurements, due to possible contributions from sea salt aerosols. The MAM to JJA increase in FMF for all sites and MAN is coherent with the month-to-month increase of AboEl-Fetouh et al. (2020), although their 550 nm arithmetic means tend to be larger (monthly binned extremes of 0.81 to 0.98). Most, or at least a significant part, of this difference is likely attributable to differences between our FMF (SDA) separation of the product and the SMF (AERONET-inversion) separation of the climatology of AboEl-Fetouh et al. (2020). The SMF is generally larger than the FMF because it tends to attribute a fraction of the CM particle size distribution and thus a fraction of the CM AOD to the FM AOD (see, for example, the 550 nm SMF vs. FMF comparisons in Sect. 4 of Kleidman et al., 2005). More discussions about the differences in terms of FMF vs. SMF and arithmetic vs. geometric statistics are available in the Supplement.

The time series of monthly mean FM, CM, and total AODs from the 10 AERONET stations (CM AOD can be inferred from the difference between total AOD and FM AOD) and the speciated AODs from MRC are provided in Fig. 2. Bias, RMSE, and r^2 verification statistics versus AERONET for monthly binned data of individual aerosol reanalysis members and the MRC are presented in Tables 2, 3, and 4, re-

spectively. The MRC is consistently biased slightly high for FM AOD across all sites and about neutral for CM AOD for most. As a result, total AOD tends to be biased slightly high, with biases ranging from 0.00 to 0.03. RMSE values range from 0.02 to 0.03 for most sites except for Bonanza Creek, Yakutsk, and Barrow with RMSE values of 0.06, 0.05, and 0.04 (driven mainly by FM variations). The r^2 values range from 0.53 to 0.84, with FM AOD r^2 values ranging from much higher to marginally higher than the CM AOD values. This is understandable as FM AOD displays large variabilities (which models are more capable of capturing), while CM AOD displays relatively low values and smaller absolute variabilities on seasonal and interannual timescales. Also, emissions of CM aerosols like dust and sea salt are driven dynamically by model or reanalysis surface winds where the surface wind dependency increases exponentially in amplitude: the simulation of this dependency has been a challenge to all global aerosol models (Sessions et al., 2015; Xian et al., 2019).

Our previous experience with multi-reanalysis and multi-model ensembles indicates, in general, that the consensus of multi-reanalyses or multi-models shows better verification scores than individual component members (Sessions et al., 2015; Xian et al., 2019, 2020). However, these studies are based on more global analyses for which the Arctic impact is relatively weak because of the sparsity of observational Arctic data. Tables 2, 3, and 4 indicate that the Arctic is rather unique inasmuch the MRC is not necessarily the top AOD-estimation performer. NAAPS-RA generally has moderately better bias, RMSE, and r^2 verification scores for the total
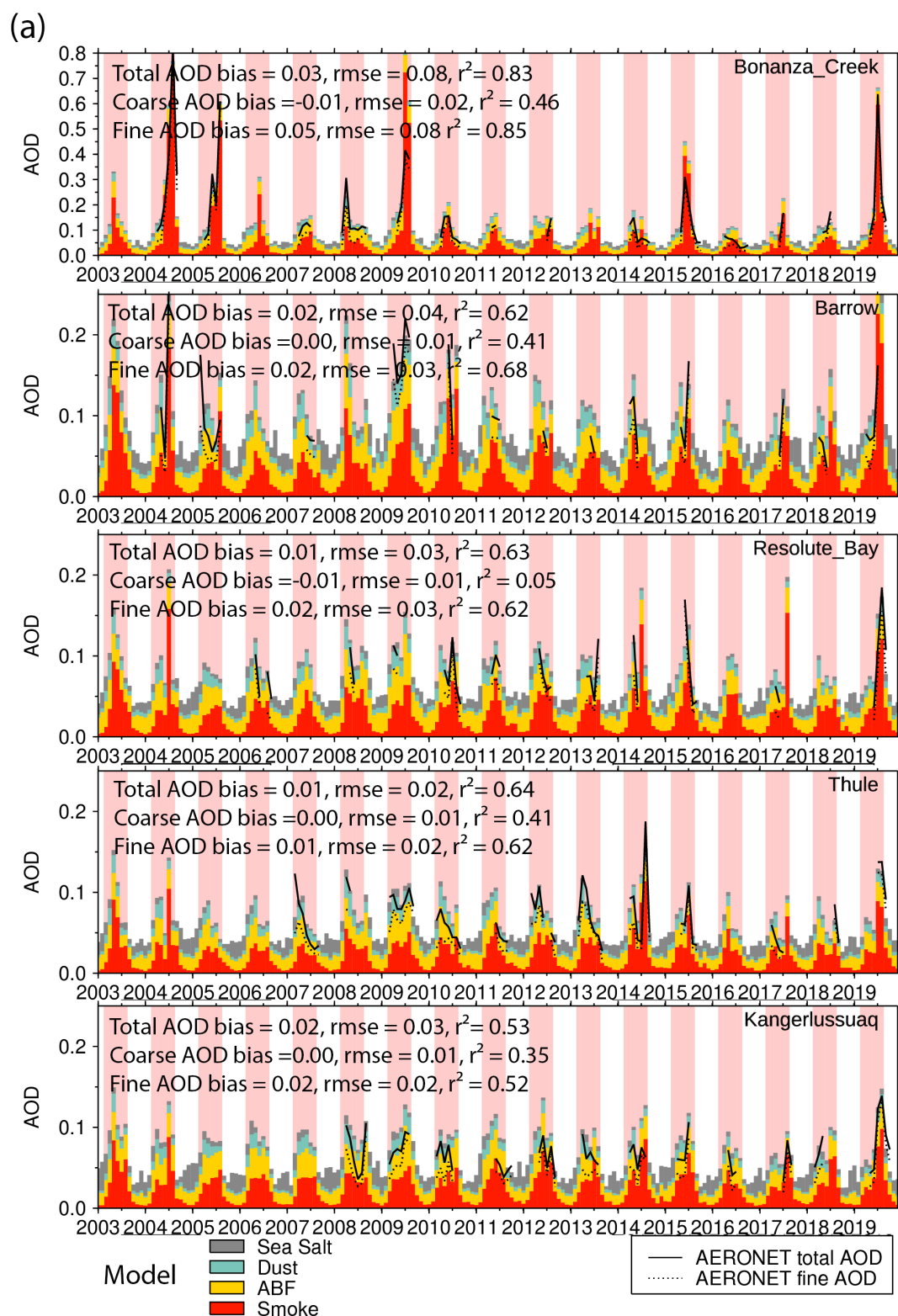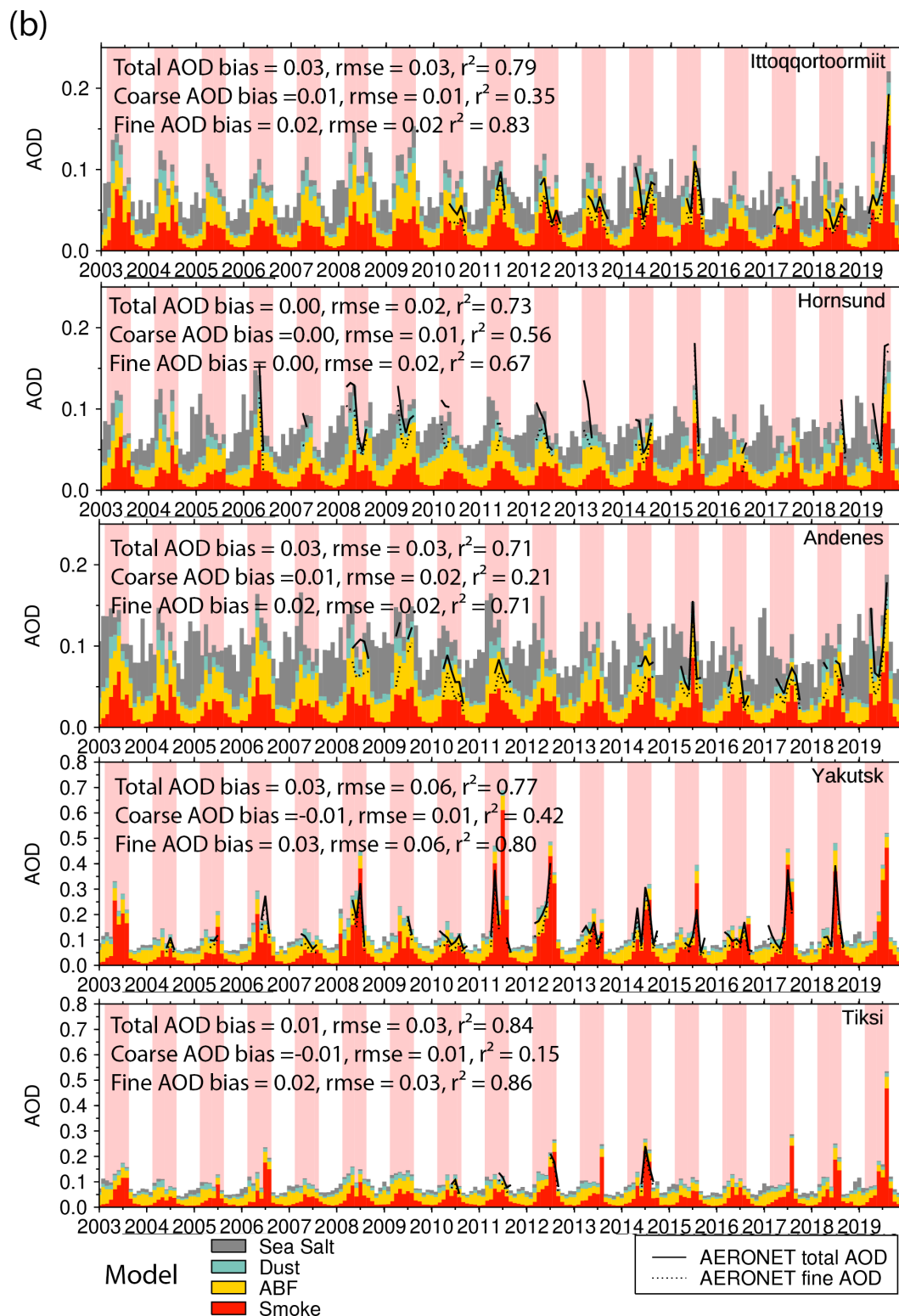
Figure 2.

Figure 2. Monthly binned time series of FM, CM, and total AERONET AODs and MRC speciated AOD at **(a)** Bonanza Creek, Barrow, Resolute_Bay, Thule, and Kangerlussuaq and **(b)** Ittoqqortoormiit, Hornsund, Andenes, Yakutsk, and Tiksi sites. The March–August periods are highlighted with pink shading for easy reading. The legends of each time series show MRC bias, RMSE, and r^2.

and FM AODs compared to MERRA-2 and CAMSRA, while CM AOD does not perform as well. In previous MRC and multi-model consensus evaluations, all component members either performed comparably in terms of AOD RMSE, bias, and r^2 or the number of multi models was relatively larger (e.g., 5 to 6 for the International Cooperative for Aerosol Prediction multi-model consensus). This study is the first time that all three developing centers have systematically evaluated their AOD reanalysis performance on an Arctic-wide climate scale.

5 Seasonal analysis

In this section we present spring and summertime Arctic AOD climatologies derived from spaceborne remote-sensing retrievals and aerosol reanalyses. We then present the seasonal cycle, interannual variability, and trends of total and speciated AODs.

5.1 Spring and summertime AOD climatology for the Arctic

5.1.1 Space-based remote-sensing AOD climatology

Bright, snow-, and ice-covered surfaces, large solar zenith angles (SZAs) and extensive cloud coverage result in limited (quality-assured) Arctic AOD retrievals from sensors like MODIS and MISR. The latitude limit of an active, downward-looking, polar-orbiting sensor like CALIOP results in a polar region profile gap above 82° N. Known CALIOP issues of retrieval filled values (RFVs) (Toth et al., 2018) and low signal-to-noise ratio over the Arctic during the summertime also limit its aerosol retrievals during the JJA season. These challenges translate to substantial data-free MAM and JJA areas in the high Arctic and Greenland as well as North America and Siberia in the MODIS, MISR, and CALIOP AOD climatology maps of Fig. 3. JJA shows significantly larger MODIS and MISR area coverage over higher latitudes as aerosol retrievals from MODIS and MISR are acquired in continuous or nearly continuous sunlight conditions. The summertime melt season means a greater presence of ice- and snow- free ocean and land surfaces as required for passive satellite-based AOD retrievals. Nevertheless, the long operation time of these sensors (about 2 decades) provides sufficient data to construct an AOD climatology as well as an emissions climatology for the near Arctic and the midlatitude regions where most sources of Arctic aerosols reside.

In general, the Fig. 3 AOD patterns are similar for all three sensors. Higher AODs of 0.15–0.25 can be observed in the 50–65° N latitude belt over land. These are associated with large boreal and subarctic areas in Siberia, east and central Europe, and North America in both spring and summer. AODs, mostly higher than 0.2 over Siberia in JJA, are associated with biomass burning events. The average AOD over water is considerably lower, ranging from 0.02 to 0.12,

with lower AOD over the North Atlantic and relatively higher AOD in the northeast Pacific influenced by outflows from the Eurasian continent. The lowest AODs (0.02–0.06) occur over the Arctic Ocean. AOD over water is slightly higher in MAM than in JJA, which is consistent with other observation-based studies within the Arctic circle (e.g., Tomasi et al., 2015). This result is possibly related to higher pollution levels from the upstream continents in MAM. CALIOP AOD exhibits spatial patterns similar to MODIS and MISR. AODs over Greenland (unique to CALIOP) range from 0.02–0.06: these minimal values are attributable to its high elevations (nearly 2 km on average). CALIOP-derived AODs over Siberia and North America are distinctively higher in JJA than in MAM. This seasonal difference (also seen by MISR) is attributable to seasonal boreal fire activities, i.e., boreal fire is generally more active in JJA than in MAM (Giglio et al., 2013). The seemingly larger JJA vs. MAM CALIOP difference over Siberia and North American as compared with MODIS and MISR could also be associated with different averaging times (2006–2019 vs. 2003–2019) as well as data sampling rate. The swath for MODIS and MISR is on the order of a few hundred to a few thousand kilometers, while the "beam diameter" for CALIPSO is on the order of 70 m (Winker et al., 2009; Colarco et al., 2014). While MODIS and MISR yield more valid retrievals during JJA than MAM, the CALIOP data sample more during MAM due to a decreased signal-to-noise ratio during the summer (see for example O'Neill et al., 2012).

5.1.2 Arctic AOD climatology derived from aerosol reanalyses

The spatial distributions of 2003–2019 mean total AOD and speciated AOD from the three aerosol reanalyses and their consensus mean for spring and summer, respectively, are shown in Figs. 4 and 5. Although there are limited AOD data available for data assimilation in the Arctic, lower-latitude AODs that are assimilation constrained can affect Arctic AOD through transport and thus exert an indirect Arctic AOD constraint. Additionally, all the reanalyses use satellite fire-hotspot-based BB emissions with a fine temporal resolution (hourly to daily). This exerts a source constraint, especially temporally (emission magnitude differs more than timing among the different models). As a result, there are significant similarities in the spatial distributions of total AODs among the three reanalyses. For example, MAM total-AOD values are, for all reanalyses, high in the 50–65° N belt over the Eurasian continent and its downwind Pacific region (values of 0.16–0.30), low (of the order of 0.1 or less) for regions north of 70° N, and at a minimum over Greenland. The high AODs over boreal North America and the Siberian BB regions are more prominent in JJA compared to MAM. In general, we would note that the distribution patterns and total-AOD magnitude are comparable to available retrievals from MODIS, MISR, and CALIOP.
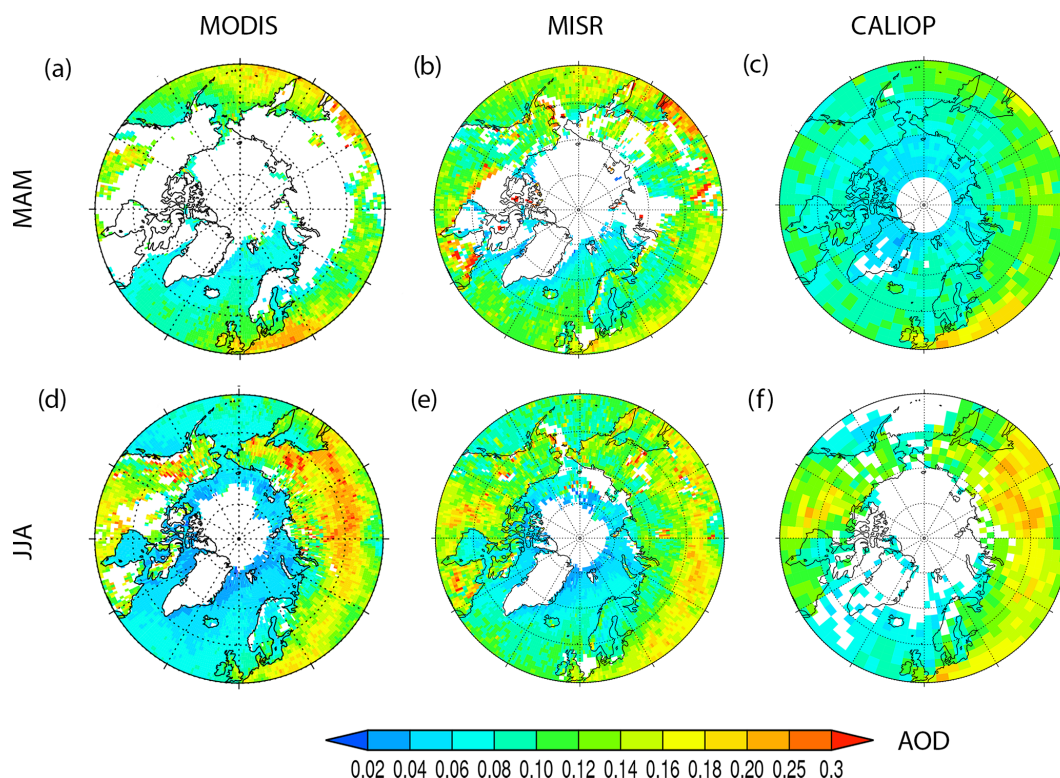
Figure 3. Satellite-derived, mean climatological MAM **(a–c)** and JJA **(d–f)** MODIS AOD at 550 nm **(a, d)**, MISR AOD at 558 nm **(b, e)**, and CALIOP AOD at 532 nm **(c, f)**. The averaging period for MODIS and MISR was 2003–2019, while the CALIOP period was 2006–2019. The white areas correspond to a lack of data. The latitude circles are at 50, 60, 70, and 80° N.

Speciated AODs have more variability than total AOD among the three reanalyses and a little more so for MAM than for JJA as shown in Figs. 4, 5, and 6. The lower JJA variability follows because passive Arctic AOD retrievals are more available in summer and reanalyses are therefore more constrained by those observations. The lower total-AOD variability is the result of it being constrained through data assimilation while speciated AOD is not: the latter AODs rely on model physics and boundary condition constraints. In general BB smoke and ABF/sulfate AODs largely dominate dust and sea salt during MAM and JJA. The MRC MAM results show similar BB smoke and ABF/sulfate magnitudes. However, the NAAPS-RA and MERRA-2 results suggest an ABF/sulfate dominance over BB smoke, while CAMSRA suggests the reverse. The high FM AOD vs. AERONET bias of CAMSRA (Table 2) suggests OM and BC and hence BB smoke overestimation. BB smoke becomes the dominant rival species over ABF/sulfate as summertime boreal BB activity increases. The increase in smoke AOD from spring to summer is a consistent feature across all the reanalyses (while CAMSRA, singularly, shows significantly higher BB smoke AOD and lower sulfate AOD in both seasons). All reanalyses show a June minimum in total AOD (Fig. 6). This is induced by general post-springtime ABF/sulfate, dust, and sea salt AOD reductions coupled with increased July and

August BB activities. The spatial distributions of seasonal mean BC AOD from MERRA-2 and CAMSRA greatly resemble those of smoke AOD (arguably more so for JJA than MAM). This suggests a dominant role of BB sources over anthropogenic BC sources over the Arctic during the spring and summer seasons. This also supports the BC emission estimate of McCarty et al. (2021) that wildfire emissions account for more than half of all BC yearly emissions north of 60° N (the authors noted much lower wintertime BB emissions when anthropogenic BC emission is at its maximum).

Figures 4, 5, and 6 indicate, for both seasons, that dust and sea salt are secondary contributors to the total AOD in the Arctic: noticeable influences of Saharan and Asian dust (see for example Stone et al., 2007; Breider et al., 2014) as well as cyclonic-induced North Atlantic Greenland Sea, Norwegian Sea, and North Pacific sea salt are observable in Fig. 4. It is also noteworthy that dust AOD in CAMSRA is much lower than the other two models (< 0.02) in the spring.

Monthly and latitudinally segmented mean AODs were found to gradually decrease from lower-latitudinal belts to higher-latitudinal belts (Fig. 7). Total AOD for the 60–70° N belt increases, on average, from MAM to JJA due to the seasonality of BB activities. However, the total AOD for the 80–90° N belt decreases slightly from MAM to JJA. This means the decreasing latitudinal gradient of total AOD is character-
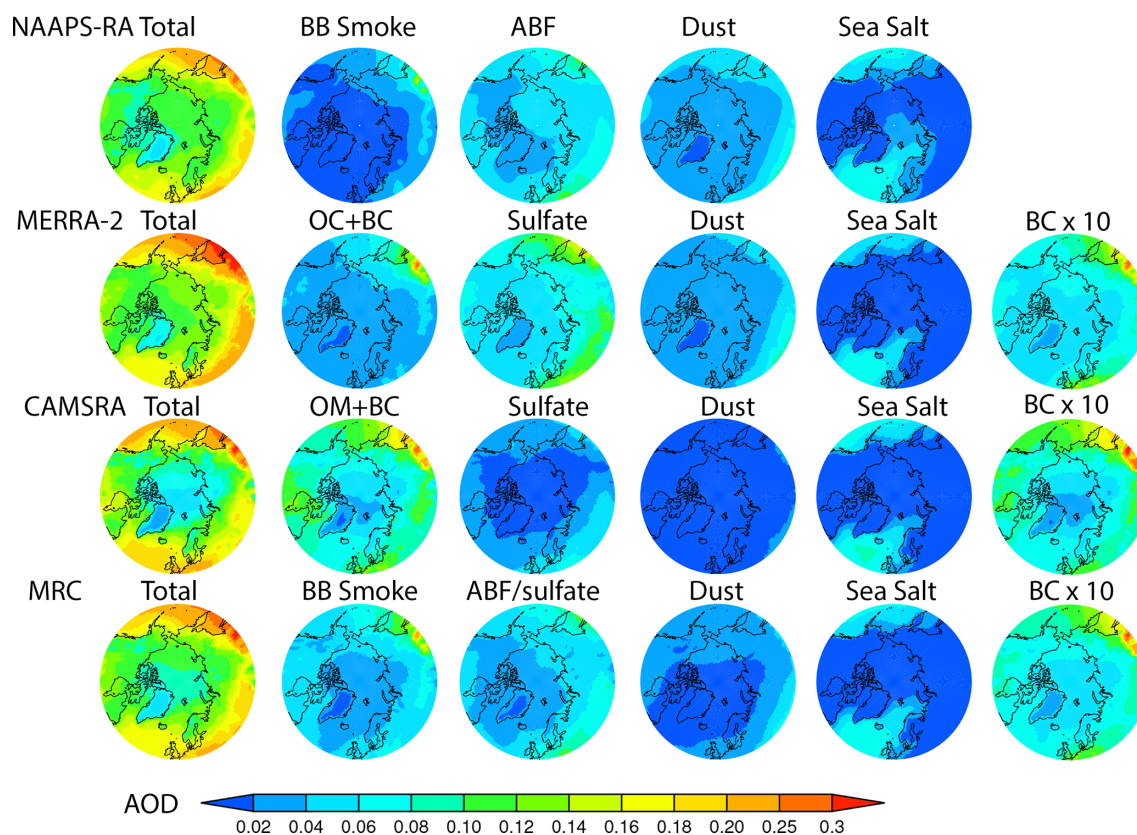
Figure 4. The 2003–2019 climatological MAM-mean total and speciated AOD at 550 nm from NAAPS-RA, MERRA-2, and CAMSRA over the Arctic.

ized by a larger amplitude in JJA than in MAM. This is most likely due to greater aerosol wet removal during transport from source regions to the high Arctic in summer (Garrett et al., 2010, 2011). It is also noted that the CAMSRA latitudinal AOD gradient is larger than those of the two other reanalyses. This suggests stronger CAMSRA aerosol removal in the Arctic compared to MERRA-2 and NAAPS-RA.

5.2 Interannual variability of AOD in the Arctic

5.2.1 General features of AOD interannual variability

As can be seen in Fig. 2 (and supported by the MAM and JJA discussion in Sect. 4), there are significant interannual AOD variabilities, especially for sites close to boreal fire sources. For example, the summertime peak of the total AERONET AOD at Bonanza Creek, Alaska, is around 0.6–0.8 in 2004, 2005, and 2019, while it is ≤ 0.1–0.2 for other years. The year-to-year factor relating high- and low-amplitude summertime peak AOD values at Yakutsk, Siberia, can be 6-fold. The MRC shows that these large interannual variabilities are fairly consistent with AERONET FM AOD variabilities and are very likely attributable to interannual variabilities in BB smoke.

For sites far from smoke sources, such as Ittoqqortoormiit on the east coast of Greenland, Hornsund in Svalbard, and Thule on the northwest coast of Greenland, the high-amplitude peak AODs are about 2–3 times the low-amplitude peak AODs. The interannual spring/summer variability is largely associated with BB smoke as suggested by the MRC and the coherent variation in the AERONET FM AOD (see for example Figs. 6 and 7). Some of the strongest AOD events reported in previous studies have been shown to be associated with the long-range transport of BB smoke. For instance, the strong AOD peak in the summer of 2015 over Hornsund and Andenes was related to a series of intense fires that originated in North America (Markowicz et al., 2016). The strong AOD peaks measured in August 2017 over Resolute Bay, Eureka, and Thule were most probably related to intense-fire-induced pyrocumulonimbus (pyroCb) events in British Columbia and the long-range transport of high-altitude smoke (Ranjbar et al., 2019; Das et al., 2021). The high-amplitude AOD peak in the spring of 2006 over Hornsund was traced to agricultural fires in eastern Europe (Stohl et al., 2007). The summer, 2004 boreal fires in North America led to the maximum-amplitude AOD peaks (Fig. 2) for the two Alaskan sites and enhanced AOD on a pan-Arctic scale (Stohl et al., 2006). Some of the high-amplitude AOD
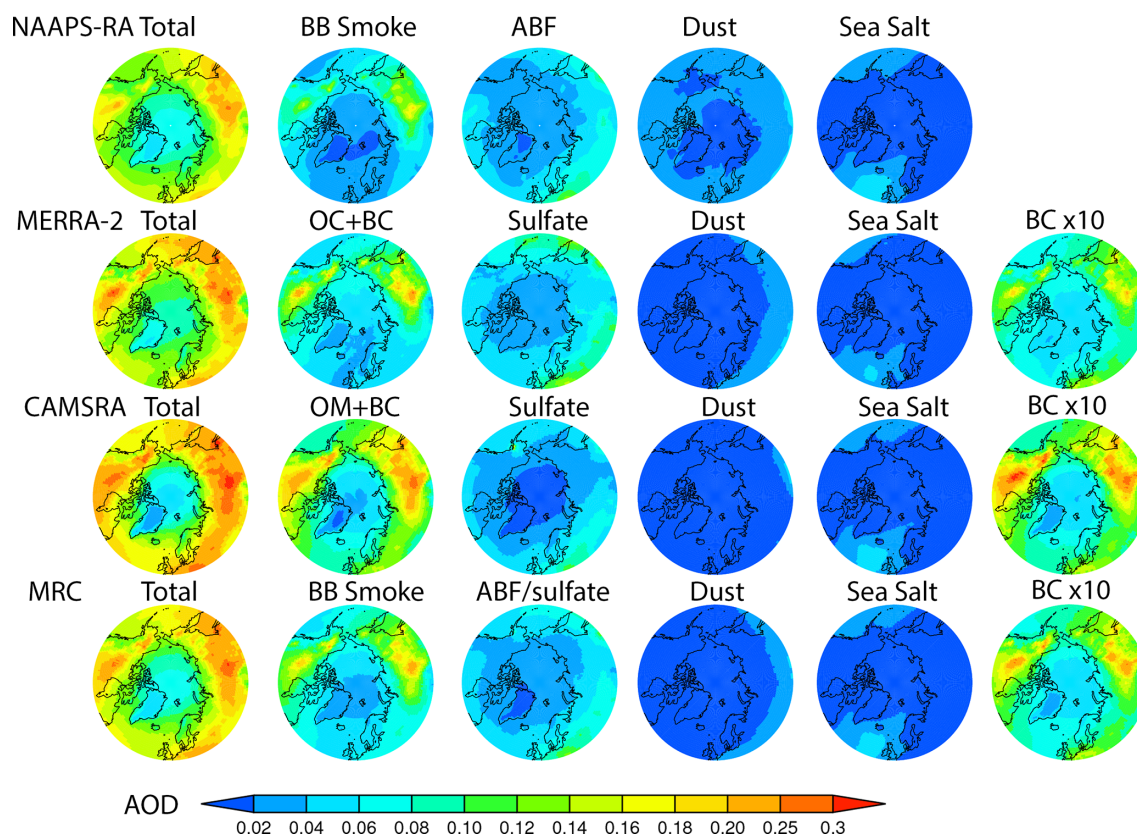
Figure 5. Same as Fig. 4 except for JJA.

peak events were recorded during intensive field campaigns. These included the Arctic Research of the Composition of the Troposphere from Aircraft and Satellites (ARCTAS), the Aerosol, Radiation, and Cloud Processes affecting Arctic Climate (ARCPAC) multi-platform campaign in the summer of 2008 (Matsui et al., 2011; Saha et al., 2010; McNaughton et al., 2011) and the NETCARE (Network on Climate and Aerosols: Addressing Key Uncertainties in Remote Canadian Environments) research vessel campaign in the spring of 2015 (Abbatt et al., 2019). Some of the BB smoke events caused short-term record-high AOD, and some lasted weeks to months, resulting in high monthly mean AOD. The statistics of extreme AOD events and implications for the impact of regional biomass burning processes are provided in Part 2 (Xian et al., 2022).

5.2.2 Attribution of AOD interannual variability

It can be observed in Fig. 6 that the simulated interannual (60–90° N) AOD variability is mostly attributable to the large interannual variability of smoke AOD (interannual variability as measured by the size of the whisker bars). This is consistent across all the reanalysis products. For March and April, the contribution from sulfate/ABF is as important as BB smoke if not larger. The interannual variation in dust

AODs, as indicated with MERRA-2 and NAAPS-RA data, is non-negligible in MAM.

Regarding spatial distribution, Fig. 8 shows the percentage of interannual variabilities of spring and summer Arctic AOD explained by different aerosol species as computed from MRC AODs for 2003–2019. The fact that both MAM and JJA interannual variabilities are mostly explained by BB smoke (maximal r^2 values) is consistent with the correlation of monthly AOD time series shown in Figs. 2 and 6. The JJA r^2 values for BB smoke are generally larger than the MAM values and lower over the North Atlantic, the Norwegian Sea, and Greenland than over the North American and Eurasian sectors. Smoke explains 60 %–80 % of MAM and, with the exception of Greenland, about 80 % of JJA AOD interannual variabilities north of 70° N. JJA values over the North American and Eurasian sectors (> 60° N) represent about 100 % explained variation. The second-largest contributor is ABF/sulfate and dust for MAM and to a lesser extent for JJA. Contribution from sea salt is weak and only statistically significant east of Greenland in JJA.

The explained variation by MAM ABF/sulfate is above 80 % over the industry- and population-concentrated European and northeast North American sectors and their outflow regions into the North Atlantic, Greenland Sea, Norwegian Sea, and the Arctic Ocean. Values decrease to above 60 %
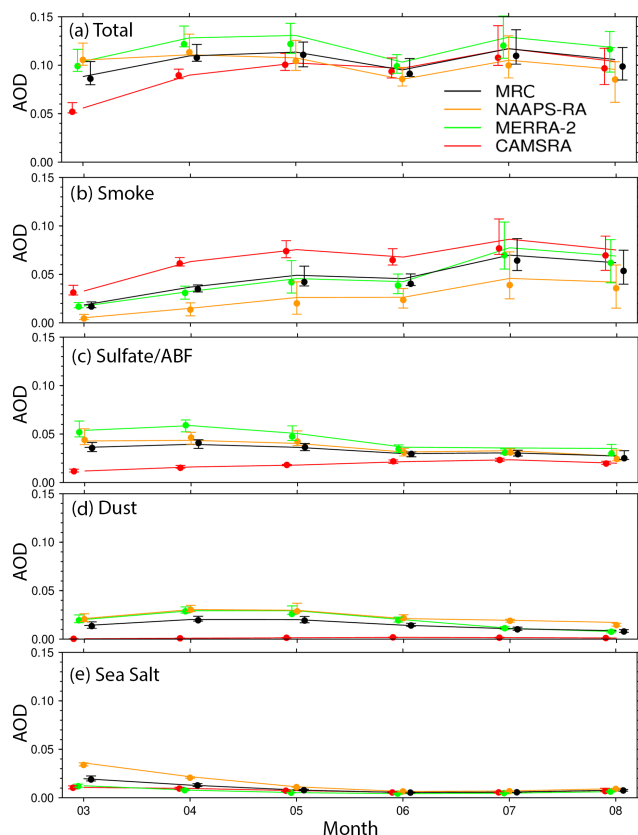
Figure 6. Climatological (2003–2019) seasonal cycle of Arctic (60–90° N) average total and speciated AODs at 550 nm from the three aerosol reanalyses and the MRC. The top and bottom whiskers and the symbols represent, respectively, the 25 % and 75 % percentiles and the medians of monthly binned AOD distributions.
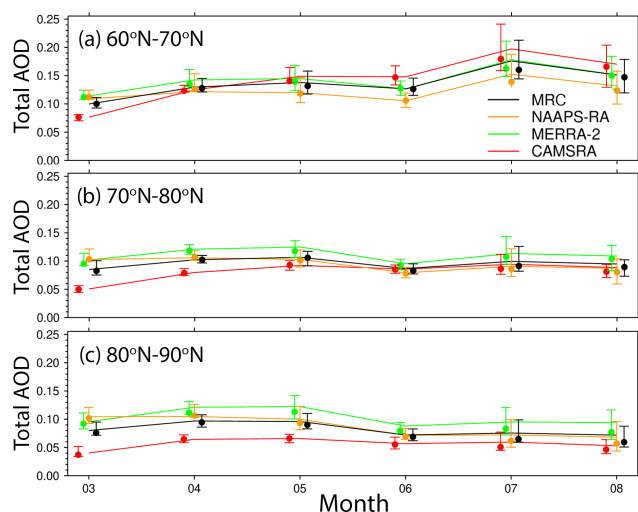
**Figure 7.** As per Fig. 6 but for total AOD and different latitudinal belts.

over Europe in general and the European Arctic (including water). Dust, possibly from Asian and high-latitude sources, could explain some of the interannual AOD variabilities over some regions (e.g., Greenland and the Greenland Sea in JJA as well as the North Pacific and the Arctic Ocean in MAM). However, there exist large uncertainties in this evaluation based on the weaker verification scores of CM compared to FM AOD (Tables 2–4), and, for example, only the CAMSRA reanalyses consider high-latitude dust. Co-variability of species, e.g., BB smoke, ABF/sulfate, and dust, is discernible in Fig. 8; this is likely due to the same transport pathways being employed from the midlatitudes to the Arctic. It is also possible that these species covary because of artifacts introduced by intrinsic treatment in AOD data assimilation for low-AOD situations (Zhang et al., 2008).

5.3 Total and speciated AOD trends over 2003–2019

The total-AOD springtime and summertime trends derived from MODIS and MISR over 2003–2019 as well 2006–2019 from CALIOP are presented in Fig. 9. Because of the scarcity of valid Arctic retrievals, valid trend analysis is mostly limited to south of 70° N and the North Atlantic region (with less MODIS and MISR coverage in MAM than in JJA and, for reasons mentioned in Sect. 5.1, less CALIOP coverage in JJA than MAM).

5.3.1 AOD springtime trends

A generally negative total-AOD MAM trend over the 50–60° N belt and the North Atlantic is shown in Fig. 9. The largest-amplitude negative trend of Fig. 9 (−0.06 to −0.10 AOD per decade) occurs over Europe; this is most likely due to a decrease in ABF/sulfate from decreased anthropogenic emissions (as we will see in the discussion surrounding the reanalyses of Fig. 10). The CALIOP trend is moderately less negative than the MODIS and MISR trends. This might, again, be attributable to the shorter length of the data record (where earlier and more polluted years of 2003–2006 for Europe and North America were not included) and/or the CALIOP daytime signal-to-noise issues. The Fig. 10 reanalyses all show a negative pan-Arctic total-AOD trend (−0.01 to −0.02 AOD per decade) except for a near-zero CAMSRA trend over the Arctic Ocean and a very slight positive trend over boreal North America. The reanalyses collectively suggest that the strong negative trend over the southeast Siberian and East Asian outflow region is associated with a decrease in BB smoke and, perhaps, a more moderate decrease in ABF/sulfate from NAAPS-RA and MERRA-2. Other consistent features shared by the reanalyses include a negative ABF/sulfate trend over Europe due to decreased anthropogenic emissions (Breider et al., 2017) and a weak positive North Atlantic sea salt trend due possibly to an observed increase in cyclonic activities (Rinke et al., 2017; Waseda et al., 2021; Valkonen et al., 2021). It is notable that NAAPS-RA
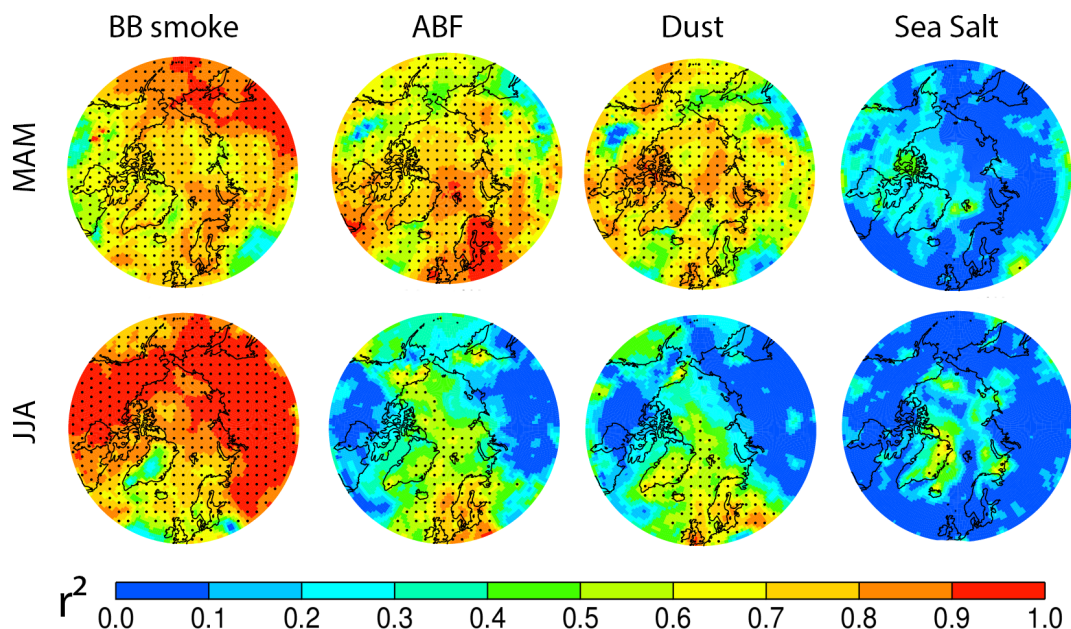
Figure 8. Percentage of interannual MRC variability of MAM (upper row) and JJA (lower row) seasonally binned, total AOD at 550 nm explained by BB smoke, ABF/sulfate, dust, and sea salt AODs. Values in dotted area are statistically significant at the 95 % level using a two-tailed Student t test.
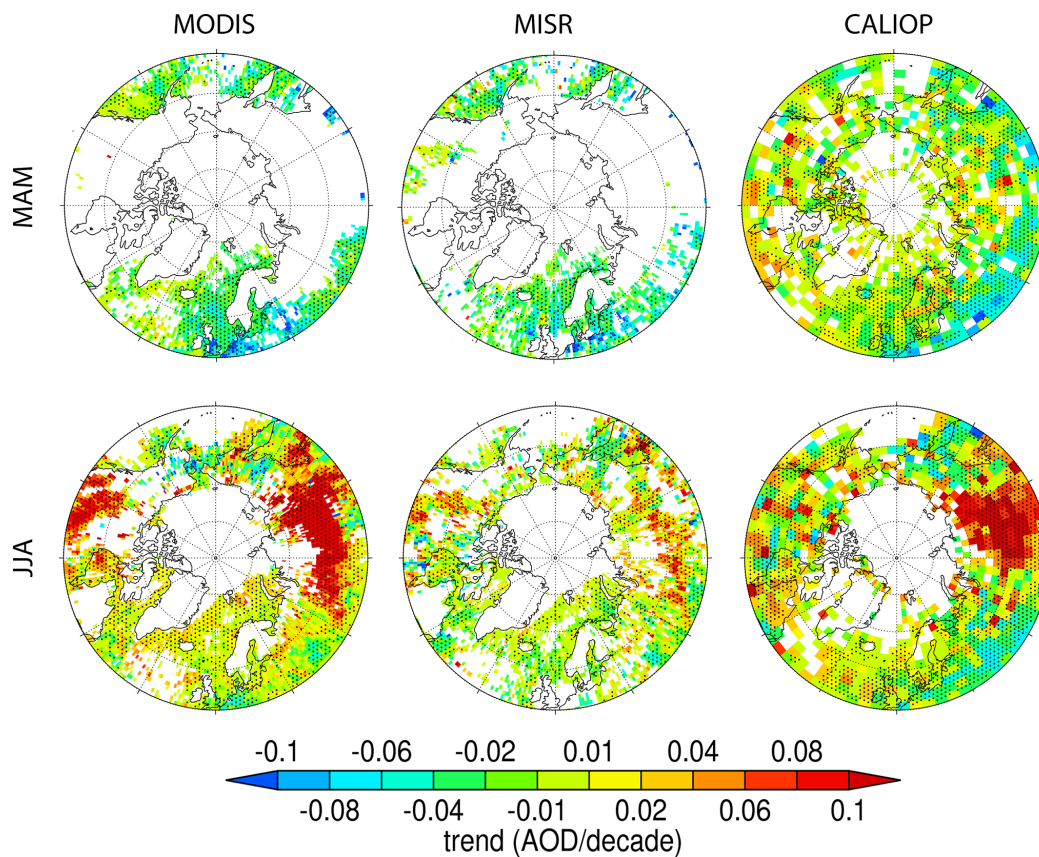
Figure 9. MODIS, MISR, and CALIOP MAM and JJA AOD trends for the time periods and AOD wavelengths given in the caption for Fig. 3. Trends in the dotted areas are statistically significant.
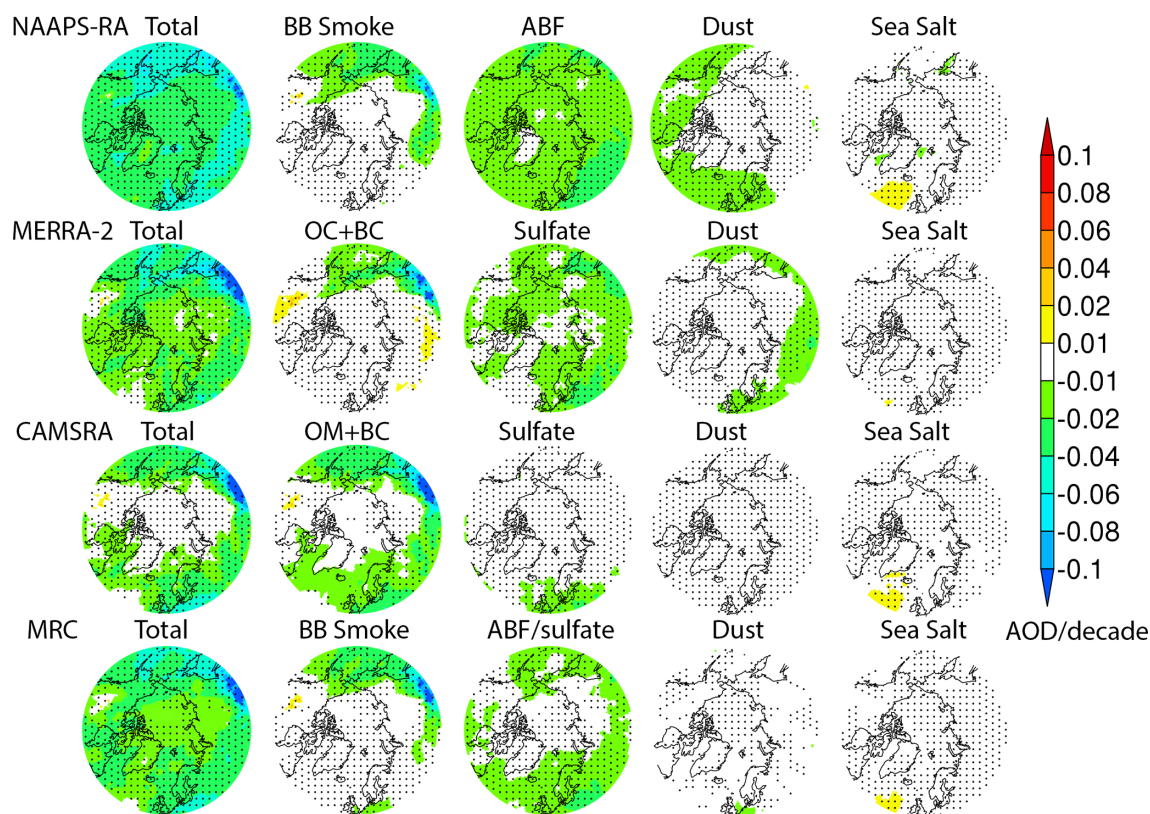
Figure 10. Trends of MAM 550 nm total AOD and contributions from BB smoke, ABF/sulfate, dust, and sea salt from NAAPS-RA, MERRA-2, CAMSRA, and the MRC for 2003–2019. Trends in the dotted areas are statistically significant.

(and MERRA-2 after 2008) do not incorporate an ABF/sulfate emission trend. This means that their ABF/sulfate trends are mostly driven by a negative AOD correction applied by the data assimilation systems. This corroborates the negative trend in ABF/sulfate.

5.3.2   AOD summertime trends

The most prominent Fig. 9 JJA feature is the strong and positive total-AOD trend (> 0.10 AOD per decade) that appears, to a varying, sensor-dependent, spatial extent, over vast regions of Siberia and North America. All the reanalyses indicate that this trend is attributable to a significant increase in BB smoke AOD (Fig. 11). This is coherent with the FLAMBE-derived, MODIS hotspot-based emission inventory of Fig. 12 that shows positive regional trends in BB emissions north of $50°$ N (and with other BB emission inventories such as GFED and GFAS inventories shown in Fig. 2 of McCarty et al., 2021). At the same time, there are negative trends in total AOD over Alaska, northeast of Russia, and the North Pacific from the reanalyses, which is seemingly consistent with the trend in remote-sensing AODs (though for some satellite datasets the coverage is spotty in these regions). These trends are driven by BB smoke and smoke emission trends as suggested by all the reanalyses and

FLAMBE. In addition, there is a continued negative trend from MAM to JJA in ABF/sulfate over Europe, which is also reflected in total-AOD trend, as shown in the reanalyses. This is consistent with the discernible negative though weak trend from the three sensors. JJA AOD trends in dust and sea salt are neutral from the reanalyses.

5.3.3   High-Arctic AOD trends

For the high Arctic, AOD trends will hardly be seen with the same color scale as those for the lower latitudes because of lower AOD. Thus, they are shown separately in Fig. 13, where time series of MAM and JJA area-mean total, smoke, and ABF/sulfate AODs are shown individually and for all the reanalyses and the MRC over the 2003–2019 time period. There is a negative trend across models in MAM total AOD with -0.017 AOD per decade (-18% per decade) and a positive trend in JJA total AOD with 0.007 AOD per decade (8% per decade) based on the MRC. The largest contributor to the MAM negative trend is ABF/sulfate, and the smoke AOD trend is also negative. In the summertime, the ABF/sulfate trend continues to be negative; however, the smoke AOD trend turns positive, with a high positive trend of 0.010 AOD per decade (22% per decade). BC AOD trends from MERRA-2 and CAMSRA are dominantly driven by smoke
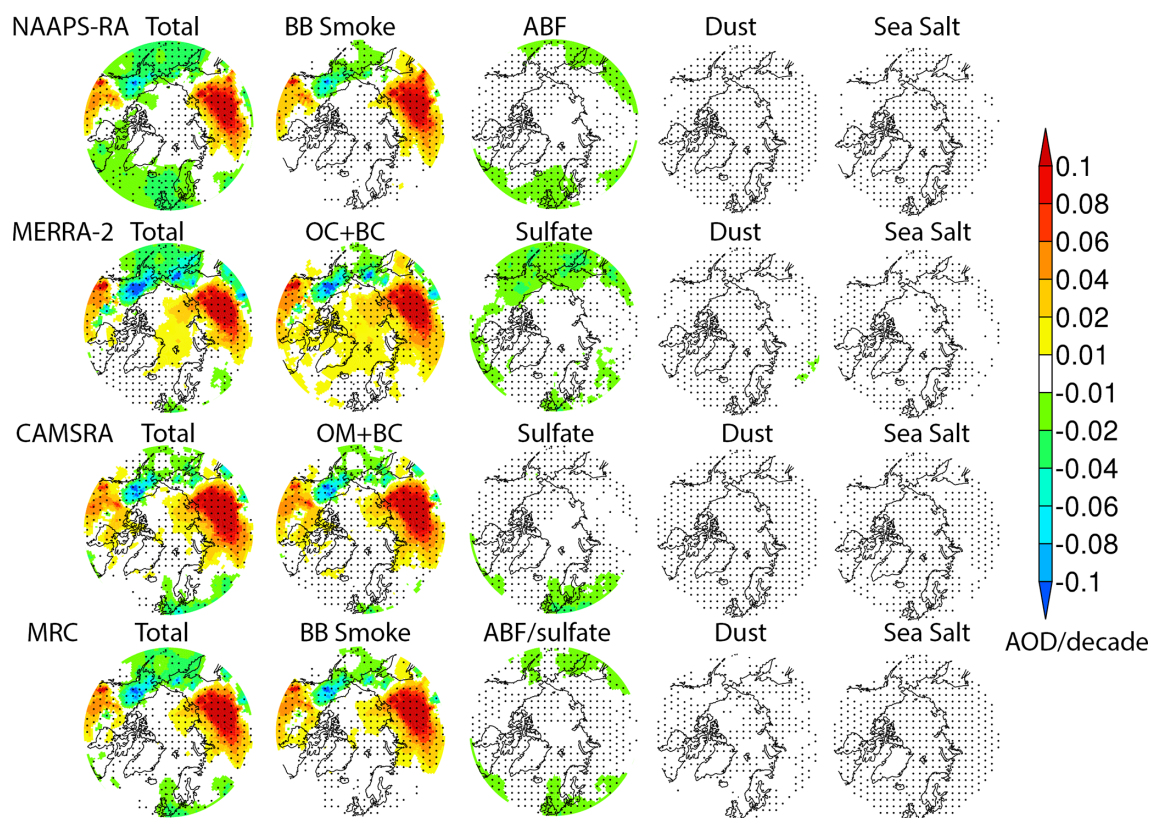
**Figure 11.** Same as Fig. 10 except for JJA.

AOD and have similar trends with smoke AOD in percentage per decade. The negative trend in ABF/sulfate AOD is in line with the decreasing trend in surface sulfate mass concentrations measured over Arctic observational sites (e.g., Breider et al., 2017). The negative trend in MAM and positive trend in JJA for smoke AOD are consistent with the seasonally binned and latitude-belt-binned mean BB emission trends shown in Fig. 12e and f. The trend magnitudes of the three aerosol reanalyses are different, but the signs are the same, corroborating the trend analysis results based on the MRC. These results are consistent with the trend analysis for lower-latitude source regions as shown in Figs. 9–11. All these results also demonstrate that the Arctic aerosol baseline is changing quickly (Schmale et al., 2021), and the estimation here could contribute to the understanding and quantification of this new baseline.

5.3.4 Possible causes of BB smoke AOD trends

Besides rising surface temperature, climate phenomena such as the El Niño–Southern Oscillation (ENSO), Arctic Oscillation (AO), and Pacific Decadal Oscillation (PDO) have been reported as affecting fire activity in several key boreal fire source regions (Balzter et al., 2007; Macias Fauria and Johnson, 2006; Kim et al., 2020). However rising surface temperature probably contributes more to the observed trend in BB

emission in the high latitudes. With the rising surface temperature, lightning activity and lightning-caused wildfires in summertime high-latitude regions were observed to increase in the past 2 decades (Z. Zhang et al., 2021; Bieniek et al., 2020; Coogan et al., 2020). In addition, agricultural fire activity in eastern Europe and European Russia (peaking at April to May) and central Asia and Asiatic Russian (peaking in August) (Korontzi et al., 2006; Hall et al., 2016) also affects the seasonality of total BB emissions. The MAM negative trend in BB smoke may be relevant to a strengthening of agriculture burning regulations in the later part of the time period. For example, the MAM BB emission maxima in 2003, 2006, and 2008 are all associated with widespread springtime agriculture burnings in high latitudes (Korontzi et al., 2006; Stohl et al., 2007; Saha et al., 2010). The aforementioned climate oscillations also modulate interannual variations in the transport of pollutants from the midlatitudes to the Arctic (e.g., Eckhardt et al., 2003; Fisher et al., 2010). Compared with the BB emission trend, the trend in the atmospheric processes, e.g., transport and removals, probably plays a secondary role in the Arctic smoke AOD trend. This is illustrated by the similarity in spatial patterns of smoke AOD and BB emission trends, and the coincidence of peak years for emissions and the high-Arctic area-mean smoke AODs. For example, 2012 and 2019 are associated with JJA peaks in emission and
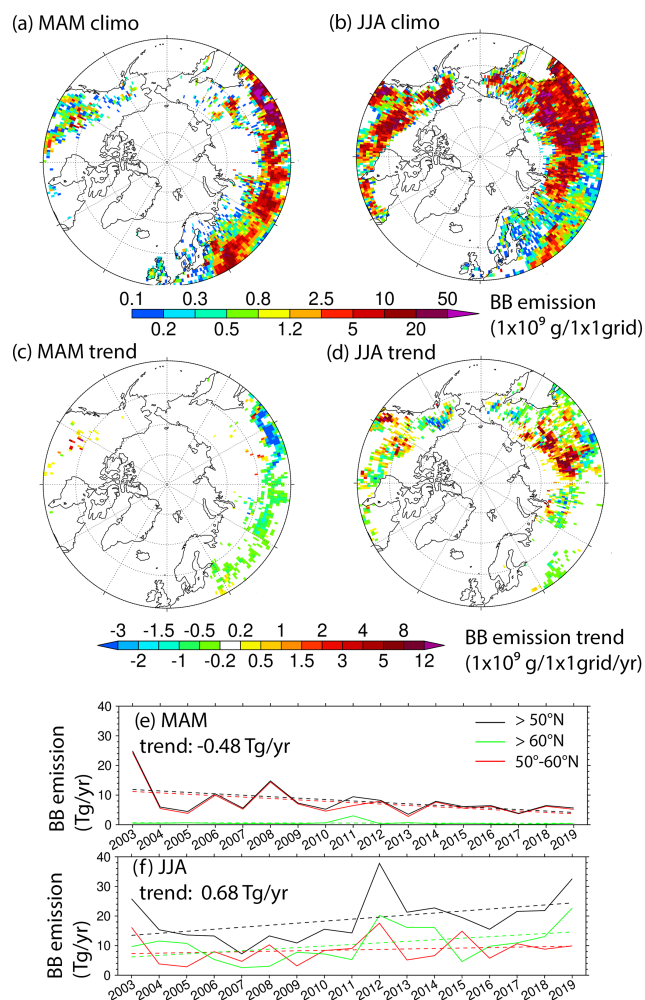
Figure 12. MAM and JJA seasonal total BB smoke particle emission climatologies and trends for 2003–2019 derived from FLAMBE. Panels **(e)** and **(f)**: time series of seasonally binned area-mean (> 50° N, > 60° N, and 50–60° N) BB smoke ($PM_{2.5}$ particle) emissions for MAM and JJA, respectively. Dashed lines represent linear trends, which are statistically significant with a confidence level of 95 %. The trend for north of 50° N is displayed in the legends.

high-Arctic smoke AOD, while 2003 and 2008 correspond to MAM peaks in both (Figs. 12 and 13).

6 Discussion

The quality control processes applied to the AOD retrievals from MODIS, MISR, and CALIOP help to generate a consistent AOD climatology and trend near the Arctic. The cloud-clearing process on the MISR data and QA processes on the MODIS data removed a good volume of data (about 40 % for MISR and MODIS). However, these QA processes help to retain only the best-quality data, which yield a closer magnitude of AOD for MODIS and MISR to AERONET

AODs near the 70° N latitude circle (around or less than 0.1), compared to ∼ 0.2 using regular level 3 MODIS and MISR data in Figs. 20 and 23 of Tomasi et al. (2015), especially for springtime. The manual QA process on the AERONET AOD data also reveals more frequent cloud contamination in springtime than in summertime. Often artificial AOD values of zero are observed over the Arctic in CALIOP V4.2 L2 and L3 data, resulting partially from algorithmically setting altitude bins with retrieval filled values in the aerosol profile to zero, as these represent undetectable levels of faint aerosol (i.e., Toth et al., 2016; 2018). With AOD = 0 values retained in the CALIOP V4.2 L2 data analysis (same processing in CALIOP V4.2 L3), the climatological seasonal mean AOD magnitude is much smaller (about half) than that shown in Fig. 3 and the AOD trends are slightly smaller than those in Fig. 9. However, the spatial patterns of the seasonal AOD and trends are similar to those obtained with AOD data after removing the AOD = 0 values (Fig. S2). After removing the pixels with filled and zero values, CALIOP AOD seasonal spatial AOD distributions are similar to those from MODIS and MISR.

The total AOD at 550 nm from the three aerosol reanalyses are much more convergent in spatial distribution, magnitude, and seasonality in the Arctic compared to the climate models and are similar to those from the remote sensors near the Arctic. For example, for AeroCom models in Sand et al. (2017), MAM AODs averaged over nine Arctic AERONET sites (all included in this study) are an order of magnitude different for the highest and lowest AOD models, and peak AOD season varies among winter, spring, and summer. In the CMIP5 models in Glantz et al. (2014), spring and summertime AODs over the Svalbard area also show an order of magnitude difference, and there are different seasonalities for some of the models. The possible reasons for the convergence of AOD in the reanalyses include the following: (1) the hourly/daily resolved satellite hotspot-based BB emissions used by these reanalyses apply fine temporal and interannual-variability-resolved emission constraints; (2) despite the commonly assimilated satellite AOD (e.g., MODIS AOD in all three reanalyses) having limited coverage in the Arctic due to retrieval challenges of dealing with bright surfaces and high cloud coverage, the observational constraint of model fields through the assimilation of AOD in the lower latitudes is effective in constraining Arctic AOD to a good extent through transport; (3) more accurate meteorology representations. It is reasonable that the AOD spread among the three reanalyses increases with latitude and into the early months (e.g., March) when retrieval coverage for lower latitudes is less than in summer months.

Except for the chemical processes relevant to conversion of SO_2 to sulfate, the aerosol reanalysis products (or their underlying aerosol models) do not include other new particle formation processes that may be important over the Arctic open-water/leads in springtime or over packed ice during the transitional summer-to-autumn season (Abbatt et al.,
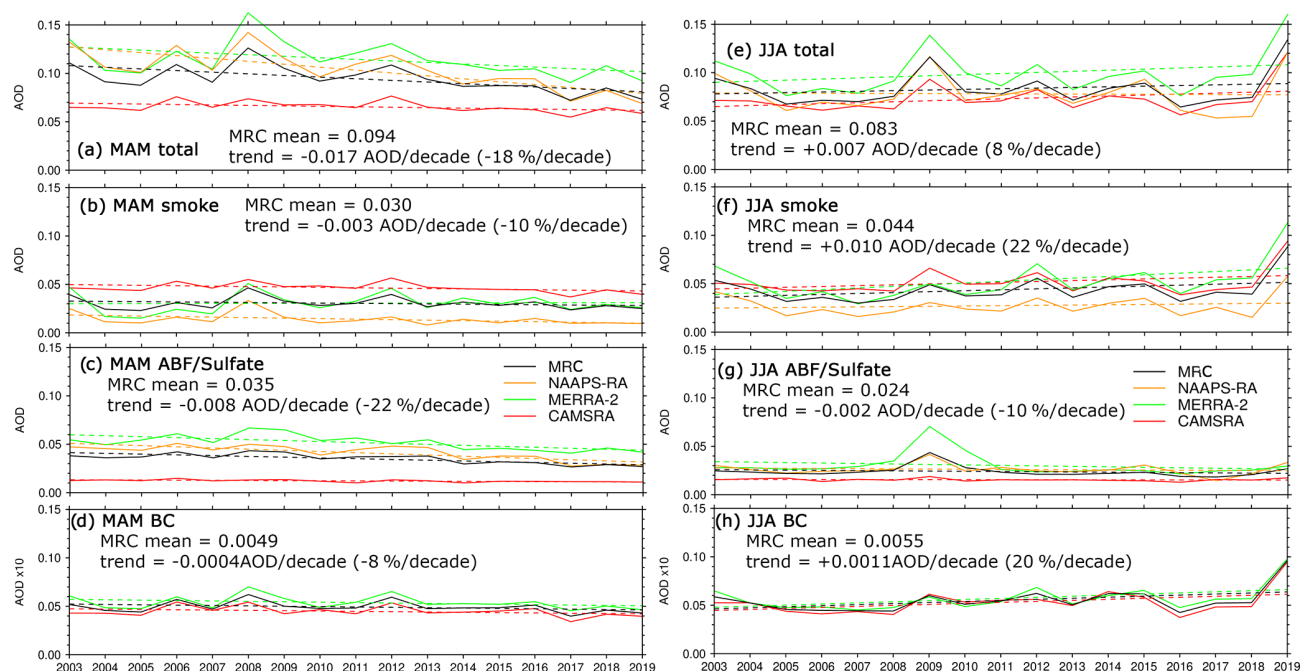
Figure 13. Time series of MAM and JJA 70–90° N area-mean total, BB smoke, ABF/sulfate, and BC AODs from the reanalyses and the MRC. Solid lines are AODs, and dashed lines are linear regressions indicating trends. For easier visualization, BC AOD is multiplied by 10.

2019; Baccarini et al., 2020). High-latitude dust sources, e.g., glacier dust, which are present for some areas in the Arctic (Bullard et al., 2016), are only included in CAMSRA, despite Arctic dust AOD in CAMSRA being much lower than those in the other two models (Fig. 6d).

To show the contribution of biomass burning on total AOD in the Arctic, we approximated BB smoke with the sum of BC and OC/OM from MERRA-2 and CAMSRA. This approximation is arguable: it is better suited for JJA than MAM, as the climatological seasonally binned mean of Arctic AOD is dominated by BB smoke in JJA. This means that BC and OC/OM are mostly from BB sources in JJA, while the contribution of BC and OC/OM from anthropogenic sources is relatively higher in early spring (Figs. 4 and 5). As a result smoke AOD is overestimated from MERRA-2 and CAMSRA and more so for MAM. This explains the larger difference in smoke AOD (ratio to total AOD) in MAM than in JJA between the two reanalyses and NAAPS-RA, which explicitly tracks aerosol mass from BB sources (Figs. 4–6). NAAPS-RA includes BC and OM from anthropogenic sources and sulfate into ABF, which is an arguably reasonable configuration for pollution species. This is because observational studies show a strong correlation between sulfate and elemental BC surface concentrations at pan-Arctic sites away from BB sources, indicating that the sources contributing to sulfate and BC are similar and that the aerosols are internally mixed and undergo similar removal (Eckhardt et al., 2015). BB smoke is expected to have different vertical distributions from anthropogenic pollution if smoke is emitted

above the boundary layer. Some estimates based on satellite observations near local noon have suggested that the fraction of smoke escaping the boundary layer is only ∼ 10 % (Val Martin et al., 2010), but taking account of the diurnal cycle of fire activity and potential for pyroconvection, the actual fraction of elevated smoke could be much larger (Fromm et al., 2010; Peterson et al., 2015, 2017).

Stratospheric aerosols from volcanic eruptions can contribute to the total AOD in the Arctic, especially for the 4 years after the Mount Pinatubo eruption in 1991 (Herber et al., 2002). For our study period, the eruptions of Kasatochi, Redoubt, Sarychev, and Eyjafjallajökull in August 2008, March 2009, July 2009, and March 2010, respectively, would have affected the stratospheric AOD and thus total-column AOD. However, these eruptions are at least 1 order of magnitude smaller than that of Pinatubo. The stratospheric AOD contribution to the Arctic background AOD is estimated to be relatively small at ∼ 0.01 (from Fig. 16 of Thomason et al., 2018; non-Pinatubo-affected years in Fig. 5 of Herber et al., 2002), despite the fact that locally and over a short period the AOD contribution can be large (e.g., O'Neill et al., 2012). All the reanalyses have some sort of SO_2 and sulfate representation from volcanic degassing emissions, but a full representation for explosive volcanic sources is lacking (except that MERRA-2 has time-varying explosive and degassing volcanic SO_2 before 31 December 2010). The volcanic influence on Arctic AOD, if detectable, would be reflected in the ABF/sulfate AOD in the reanalyses, but its contribution would be much smaller than the anthropogenic

counterpart for our study period. It is also worth noting that volcanic activities are not the only influence on the stratospheric aerosol budget: pyroCB-injected BB smoke can also contribute to stratospheric AOD, as discussed earlier. Stratospheric BB smoke was also detected over the Arctic with lidar measurements during the MOSAiC campaign (Engelmann et al., 2021). Stratospheric injection of BB smoke associated with pyroCB events is not represented in the reanalyses, despite BB emission associated with these pyroCB events being included in the emission inventories with a possible large bias in emission amount and height.

Arctic shipping is often brought up as a potentially important source of BC for the Arctic in the future. All of the reanalyses include shipping emissions, although little interannual trend is considered especially for the late period in 2003–2019. However "Arctic shipping is currently only a minor source of black carbon emissions overall" according to the recent Arctic Monitoring and Assessment Programme (AMAP) report (AMAP, 2021).

7 Conclusions

Using remote-sensing AOD retrievals from MODIS, MISR, and CALIOP and AODs from three aerosol reanalyses, including NAAPS-RA, MERRA-2, and CAMSRA, and ground-based AERONET data, we have reported the Arctic/high-Arctic AOD climatology and trend for spring and summer seasons during 2003–2019.

1. *Arctic AOD climatology*. The total AODs from spaceborne remote sensing and the aerosol reanalyses show quite consistent climatological spatial patterns and interannual trends for both spring and summer seasons for the lower Arctic, where remote-sensing data are available. AOD trends for the high Arctic from the reanalyses have consistent signs too. Climatologically, FM AOD dominates CM AOD in the Arctic. Based on the reanalyses, BB smoke AOD increases from March to August associated with a seasonality of BB activities in the boreal region ($> 50°$ N); ABF/sulfate AOD is slightly higher in MAM than in JJA; sea salt AOD is highest in March and decreases with time into later spring and summer; the contribution of dust AOD to total AOD is non-negligible in April and May. The latitudinal gradient of AOD is larger in JJA than in MAM, consistent with observed more efficient removal in summertime (Garrett et al., 2011). Among aerosol species, BC is a very efficient light absorber and climate forcing agent (e.g., Bond et al., 2013). We show that over the Arctic, the contribution of BC AOD from BB source overwhelms anthropogenic sources in both MAM and JJA and more so in JJA during 2003–2019.

2. *Interannual AOD trend*. Total AOD exhibits a general negative trend in the Arctic in MAM and strong positive

trends in North America and Eurasian boreal regions (except Alaska and northeast Siberia) in JJA. For the high Arctic, the total-AOD trend is -0.017 per decade (-18 % per decade) for MAM and 0.007 per decade (8 % per decade) for JJA based on the MRC. The total-AOD trends are driven by an overall decrease in sulfate/ABF AOD in both seasons (-0.008 per decade or -22 % per decade for MAM and -0.002 per decade or -10 % per decade for JJA) and a negative trend in MAM (-0.003 per decade or -10 % per decade) and a strong positive trend in JJA (0.01 per decade or 22 % per decade) from biomass burning smoke AOD. The decreasing trend in sulfate in the Arctic in recent decades is in line with other studies using surface concentration measurements (e.g., Eckhardt et al., 2015). The smoke AOD trends are consistent with MODIS fire-hotspot-based BB emission trends over the boreal continents.

3. *Impact of BB smoke on AOD interannual variability*. The interannual variability of total AOD in the Arctic is substantial and predominantly driven by fine-mode and, specifically, BB smoke AOD in both seasons and more so in JJA than in MAM. For AERONET sites close to BB emission sources, the difference in monthly total AOD can be 6-fold for high- versus low-AOD years. For remote regions away from BB sources, the interannual variability of total AOD can also be explained mostly by smoke AOD.

4. *Overall performance of the aerosol reanalyses*. The aerosol reanalyses yield much more convergent AOD results than the climate models (e.g., AeroCom models in Sand et al., 2017; CMIP5 models in Glantz et al., 2014) and are verified with AERONET to some good extent, which corroborates the climatology and trend analysis. Speciated AODs appear more diverse than the total AOD among the three reanalyses and a little more so for MAM than for JJA. NAAPS-RA and MERRA-2 total and FM AODs are verified better in the Arctic than CAMSRA, which tends to have a high bias in FM overall. The reanalyses generally perform better in FM than CM. The three reanalyses exhibit different latitudinal AOD gradients, especially in summertime, indicating different removal efficiencies. The emerging capability of assimilating the Ozone Monitoring Instrument (OMI) aerosol index (AI) to constrain absorptive aerosol amount could potentially fill in the observational gaps for aerosol data assimilation in reanalyses over the Arctic (J. Zhang et al., 2021). With more advanced retrieval algorithms on the current spaceborne sensors over snow/ice, new sensors on future satellites, and improvements to the underlying meteorology and aerosol representations in models, improvements in aerosol reanalysis are expected.

The results presented here provide a baseline of AOD spatiotemporal distribution, magnitude, and speciation over the Arctic during the spring and summer seasons for the recent 2 decades. This will help improve aerosol model evaluations and better constrain aerosol radiative and potentially indirect forcing calculation to evaluate aerosol impact in the Arctic amplification. For example, the contribution of reduction in sulfate to Arctic surface warming in recent decades (e.g., Shindell and Faluvegi, 2009; Breider et al., 2017) could potentially be better quantified, with the caveat that speciated AOD has larger uncertainties than total AOD in the reanalyses. The AOD statistics could also provide background information for field campaign data analysis and future field campaign planning in a larger climate context. It is also recommended that climate models should take into account BB emissions besides anthropogenic climate forcers and BB interannual variabilities and trends in Arctic climate change studies.

Appendix A

Table A1. Summary of data used in the study.

Products	Data	Resolution	Time
MODIS (Moderate Resolution Imaging Spectroradiometer) C6.1L3	550 nm AOD	1° × 1° monthly	2003–2019
MISR (Multi-angle Imaging SpectroRadiometer) V23	558 nm AOD	1° × 1°, monthly	2003–2019
CALIOP (Cloud-Aerosol Lidar with Orthogonal Polarization) V4.2L2	532 nm AOD	2° × 5°, monthly	2006–2019
AERONET (AErosol RObotic NETwork) V2L3	SDA total, FM, CM AOD at 550 nm	6-hourly, monthly	2003–2019
MAN (Marine Aerosol Network) Level2	SDA total, FM, CM AOD at 550 nm	6-hourly	2003–2019
MERRA-2 (Modern-Era Retrospective Analysis for Research and Applications, v2)	Total and speciated AOD at 550 nm	0.5° lat × 0.63° long, monthly	2003–2019
CAMSRA (Copernicus Atmosphere Monitoring Service Reanalysis)	Total and speciated AOD at 550 nm	0.7° × 0.7°, monthly	2003–2019
NAAPS-RA v1 (Navy Aerosol Analysis and Prediction System reanalysis v1)	Total and speciated AOD at 550 nm	1° × 1°, monthly	2003–2019
MRC (Multi-Reanalysis-Consensus)	Total and speciated AOD at 550 nm	1° × 1°, monthly	2003–2019
FLAMBE (Fire Locating and Modeling of Burning Emissions) v1.0	BB smoke emission flux	1° × 1°, monthly	2003–2019

Note: these are the final form of data used in this study. Some pre-processing and quality control were applied to remote-sensing data as described in Sect. 2.

Code and data availability. All data supporting the conclusions of this paper are available either through the links provided below or upon request.

- AERONET Version 3 Level 2 data: http://aeronet.gsfc.nasa.gov (last access: 10 July 2022; AERONET, 2022).

- MAN data: https://aeronet.gsfc.nasa.gov/new_web/maritime_aerosol_network.html (last access: 10 July 2022, NASA, 2022a).

- MODIS data-assimilation-quality AOD: https://doi.org/10.5067/MODIS/MCDAODHD.NRT.061 (The Naval Research Laboratory and the University of North Dakota/MODIS Adaptive Processing System (MODAPS), 2017).

- MISR AOD: https://doi.org/10.5067/TERRA/MISR/MIL2ASAE_L2.003-23 (NASA, 2022b).

- CALIOP from NASA Langley Research Center Atmospheric Science Data Center: https://doi.org/10.5067/CALIOP/CALIPSO/LID_L2_05kmAPro-Standard-V4-20 (NASA/LARC/SD/ASDC, 2018a) for the Version 4.2 CALIPSO Level 2 5 km aerosol profile and https://doi.org/10.5067/CALIOP/CALIPSO/LID_L2_05kmALay-Standard-V4-20 (NASA/LARC/SD/ASDC, 2018b) for aerosol layer products. Further quality-assured data are available upon request.

- NAAPS RA AOD: https://usgodae.org/cgi-bin/datalist.pl?Data_Type=naaps&Parameter=ALL&Provider=ALL&meta=Go (last access: 10 July 2022).

- MERRA-2 AOD: https://doi.org/10.5067/FH9A0MLJPC7N (Global Modeling and Assimilation Office, 2015).

- CAMSRA AOD: https://www.ecmwf.int/en/research/climate-reanalysis/cams-reanalysis (last access: 10 July 2022).

- The FLAMBE BB smoke inventory is available upon request from U.S. NRL.

Supplement. The supplement related to this article is available online at: https://doi.org/10.5194/acp-22-9915-2022-supplement.

Author contributions. PX and JZ designed this study. PX performed most of the data analysis and wrote the initial paper. TDT, BS, and EJH helped with processing of CALIOP, MISR, and MODIS AOD data, respectively. All authors contributed to scientific discussion, writing, and revision of the paper.

Competing interests. The contact author has declared that none of the authors has any competing interests.

Disclaimer. Publisher's note: Copernicus Publications remains neutral with regard to jurisdictional claims in published maps and institutional affiliations.

Review statement. This paper was edited by Hailong Wang and reviewed by two anonymous referees.

References

Abbatt, J. P. D., Leaitch, W. R., Aliabadi, A. A., Bertram, A. K., Blanchet, J.-P., Boivin-Rioux, A., Bozem, H., Burkart, J., Chang, R. Y. W., Charette, J., Chaubey, J. P., Christensen, R. J., Cirisan, A., Collins, D. B., Croft, B., Dionne, J., Evans, G. J., Fletcher, C. G., Galí, M., Ghahremaninezhad, R., Girard, E., Gong, W., Gosselin, M., Gourdal, M., Hanna, S. J., Hayashida, H., Herber, A. B., Hesaraki, S., Hoor, P., Huang, L., Hussherr, R., Irish, V. E., Keita, S. A., Kodros, J. K., Köllner, F., Kolonjari, F., Kunkel, D., Ladino, L. A., Law, K., Levasseur, M., Libois, Q., Liggio, J., Lizotte, M., Macdonald, K. M., Mahmood, R., Martin, R. V., Mason, R. H., Miller, L. A., Moravek, A., Mortenson, E., Mungall, E. L., Murphy, J. G., Namazi, M., Norman, A.-L., O'Neill, N. T., Pierce, J. R., Russell, L. M., Schneider, J., Schulz, H., Sharma, S., Si, M., Staebler, R. M., Steiner, N. S., Thomas, J. L., von Salzen, K., Wentzell, J. J. B., Willis, M. D., Wentworth, G. R., Xu, J.-W., and Yakobi-Hancock, J. D.: Overview paper: New insights into aerosol and climate in the Arctic, Atmos. Chem. Phys., 19, 2527–2560, https://doi.org/10.5194/acp-19-2527-2019, 2019.

AboEl-Fetouh, Y., O'Neill, N. T., Ranjbar, K., Hesaraki, S., Abboud, I., and Sobolewski, P. S.: Climatological-scale analysis of intensive and semi-intensive aerosol parameters derived from AERONET retrievals over the Arctic, J. Geophys. Res.-Atmos., 125, e2019JD031569, https://doi.org/10.1029/2019JD031569, 2020.

AERONET: AERONET AOD Version 3 Level 2 data, http://aeronet.gsfc.nasa.gov, curator David M. Giles, AERONET [data set], last access: 10 July 2022.

AMAP: Impacts of Short-lived Climate Forcers on Arctic Climate, Air Quality, and Human Health. Summary for Policy-makers, Arctic Monitoring and Assessment Programme (AMAP), Tromsø, Norway, 20 pp., 2021.

Baccarini, A., Karlsson, L., Dommen, J., Duplessis, P., Vüllers, J., Brooks, I. M., Saiz-Lopez, A., Salter, M., Tjernström, M., Baltensperger, U., Zieger P., and Schmale, J.: Frequent new particle formation over the high Arctic pack ice by enhanced iodine emissions, Nat. Commun., 11, 4924, https://doi.org/10.1038/s41467-020-18551-0, 2020.

Baibakov, K., O'Neill, N. T., Ivanescu, L., Duck, T. J., Perro, C., Herber, A., Schulz, K.-H., and Schrems, O.: Synchronous polar winter starphotometry and lidar measurements at a High Arctic station, Atmos. Meas. Tech., 8, 3789–3809, https://doi.org/10.5194/amt-8-3789-2015, 2015.

Balmes, K. A., Fu, Q., and Thorsen, T. J.: The diurnal variation of the aerosol optical depth at the ARM SGP site, Earth Space Sci., 8, e2021EA001852, https://doi.org/10.1029/2021EA001852, 2021.

Balzter, H., Gerard, F., George, C., Weedon, G., Grey, W., Combal, B., Bartholome, E., Bartalev, S., and Los, S.: Coupling of vegetation growing season anomalies and fire activity with hemispheric and regional-scale climate patterns in central and east Siberia, J. Climate, 20, 3713–3729, 2007.

Bieniek, P. A., Bhatt, U. S., York, A., Walsh, J. E., Lader, R., Strader, H., Ziel, R., Jandt, R. R., and Thoman, R. L.: Lightning Variability in Dynamically Downscaled Simulations of Alaska's Present and Future Summer Climate, J. Appl. Meteorol. Climatol., 59, 1139–1152, 2020.

Birch, C. E., Brooks, I. M., Tjernström, M., Shupe, M. D., Mauritsen, T., Sedlar, J., Lock, A. P., Earnshaw, P., Persson, P. O. G., Milton, S. F., and Leck, C.: Modelling atmospheric structure, cloud and their response to CCN in the central Arctic: ASCOS case studies, Atmos. Chem. Phys., 12, 3419–3435, https://doi.org/10.5194/acp-12-3419-2012, 2012.

Boisvert, L. N., Petty, A. A., and Stroeve, J. C.: The Impact of the Extreme Winter 2015/16 Arctic Cyclone on the Barents–Kara Seas, Mon. Weather Rev., 144, 4279–4287, https://doi.org/10.1175/mwr-d-16-0234.1, 2016.

Bossioli, E., Sotiropoulou, G., Methymaki, G., and Tombrou, M.: Modeling extreme warm-air advection in the Arctic during summer: The effect of mid-latitude pollution inflow on cloud properties, J. Geophys. Res.-Atmos., 126, e2020JD033291, https://doi.org/10.1029/2020JD033291, 2021.

Breider, T. J., Mickley, L. J., Jacob, D. J., Wang, Q., Fisher, J. A., Chang, R. Y. W., and Alexander, B.: Annual distributions and sources of Arctic aerosol components, aerosol optical depth, and aerosol absorption, J. Geophys. Res.-Atmos., 119, 4107–4124, https://doi.org/10.1002/2013JD020996, 2014.

Breider, T. J., Mickley, L. J., Jacob, D. J., Ge, C., Wang, J., Payer Sulprizio, M., Croft, B., Ridley, D. A., McConnell, J. R., Sharma, S., Husain, L., Dutkiewicz, V. A., Eleftheriadis, K., Skov, H., and Hopke, P. K.: Multidecadal trends in aerosol radiative forcing over the Arctic: Contribution of changes in anthropogenic aerosol to Arctic warming since 1980, J. Geophys. Res.-Atmos., 122, 3573–3594, https://doi.org/10.1002/2016JD025321, 2017.

Buchard, V., Randles, C. A., da Silva, A. M., Darmenov, A., Colarco, P. R., Govindaraju, R., Ferrare, R., Hair, J., Beyersdorf, A. J., Ziemba, L. D., and Yu, H.: The MERRA-2 Aerosol Reanalysis, 1980 Onward. Part II: Evaluation and Case Studies, J. Climate, 6851–6872, https://doi.org/10.1175/JCLI-D-16-0613.1, 2017.

Bullard, J. E., Baddock, M., Bradwell, T., Crusius, J., Darlington, E., Gaiero, D., Gasso, S., Gisladottir, G., Hodgkins, R., McCulloch, R., McKenna-Neuman, C., Mockford, T., Stewart, H., and Thorsteinsson, T.: High-latitude dust in the Earth system, Rev. Geophys., 54, 447–485, https://doi.org/10.1002/2016RG000518, 2016.

Campbell, J. R., Tackett, J. L., Reid, J. S., Zhang, J., Curtis, C. A., Hyer, E. J., Sessions, W. R., Westphal, D. L., Prospero, J. M., Welton, E. J., Omar, A. H., Vaughan, M. A., and Winker, D. M.: Evaluating nighttime CALIOP 0.532 µm aerosol optical depth and extinction coefficient retrievals, Atmos. Meas. Tech., 5, 2143–2160, https://doi.org/10.5194/amt-5-2143-2012, 2012.

Chin, M., Rood, R. B., Lin, S. J., Muller, J. F., and Thompson, A. M.: Atmospheric sulfur cycle simulated in the global model GOCART: Model description and global properties, J. Geophys. Res.-Atmos., 105, 24671–24687, 2000.

Colarco, P., da Silva, A., Chin, M., and Diehl, T.: Online simulations of global aerosol distributions in the NASA GEOS-4 model and comparisons to satellite and ground-based aerosol optical depth, J. Geophys. Res., 115, D14207, https://doi.org/10.1029/2009jd012820, 2010.

Colarco, P. R., Kahn, R. A., Remer, L. A., and Levy, R. C.: Impact of satellite viewing-swath width on global and regional aerosol optical thickness statistics and trends, Atmos. Meas. Tech., 7, 2313–2335, https://doi.org/10.5194/amt-7-2313-2014, 2014.

Comiso, J. C.: Large Decadal Decline of the Arctic Multiyear Ice Cover, J. Climate, 25, 1176–1193, https://doi.org/10.1175/JCLI-D-11-00113.1, 2012.

Coogan, S. C. P., Cai, X., Jain, P., and Flannigan, M. D.: Seasonality and trends in human- and lightning-caused wildfires ≥ 2 ha in Canada, 1959–2018, Int. J. Wildland Fire, 29, 473–485, https://doi.org/10.1071/WF19129, 2020.

Coopman, Q., Garrett, T. J., Finch, D. P., and Riedi, J.: High sensitivity of arctic liquid clouds to long-range anthropogenic aerosol transport, Geophys. Res. Lett., 45, 372–381, https://doi.org/10.1002/2017GL075795, 2018.

Dai, A., Luo, D., Song, M., and Liu, J.: Arctic amplification is caused by sea-ice loss under increasing CO_2, Nat. Commun., 10, 121, https://doi.org/10.1038/s41467-018-07954-9, 2019.

Dall'Osto, M., Beddows, D. C. S., Tunved, P., Krejci, R., Ström, J., Hansson, H.-C., Yoon, Y. J., Park, Ki-Tae, Becagli, S., Udisti, R., Onasch, T., O'Dowd, C. Simó, R., and Harrison, R. M.: Arctic sea ice melt leads to atmospheric new particle formation, Sci. Rep.-UK, 7, 3318, https://doi.org/10.1038/s41598-017-03328-1, 2017.

Dang, C., Warren, S. G., Fu, Q., Doherty, S. J., Sturm, M., and Su, J.: Measurements of light-absorbing particles in snow across the Arctic, North America, and China: Effects on surface albedo, J. Geophys. Res.-Atmos., 122, 10149–10168, https://doi.org/10.1002/2017JD027070, 2017.

Das, S., Colarco, P. R., Oman, L. D., Taha, G., and Torres, O.: The long-term transport and radiative impacts of the 2017 British Columbia pyrocumulonimbus smoke aerosols in the stratosphere, Atmos. Chem. Phys., 21, 12069–12090, https://doi.org/10.5194/acp-21-12069-2021, 2021.

DeRepentigny, P., Jahn, A., Holland, M., Fasullo, J., Lamarque, J.-F., Hannay, C., Mills, M., Bailey, D., Tilmes, S., and Barrett, A.: Impact of CMIP6 biomass burning emissions on Arctic sea ice loss, EGU General Assembly 2021, online, 19–

30 April 2021, EGU21-9020, https://doi.org/10.5194/egusphere-egu21-9020, 2021.

Doherty, S. J., Warren, S. G., Grenfell, T. C., Clarke, A. D., and Brandt, R. E.: Light-absorbing impurities in Arctic snow, Atmos. Chem. Phys., 10, 11647–11680, https://doi.org/10.5194/acp-10-11647-2010, 2010.

Eck, T. F., Holben, B. N., Reid, J. S., Sinyuk, A., Hyer, E. J., O'Neill, N. T., Shaw, G. E., Vande Castle, J. R., Chapin, F. S., Dubovik, O., Smirnov, A., Vermote, E., Schafer, J. S., Giles, D., Slutsker, I., Sorokine, M., and Newcomb, W. W.: Optical properties of boreal region biomass burning aerosols in central Alaska and seasonal variation of aerosol optical depth at an Arctic coastal site, J. Geophys. Res.-Atmos., 114, D11201, https://doi.org/10.1029/2008JD010870, 2009.

Eckhardt, S., Stohl, A., Beirle, S., Spichtinger, N., James, P., Forster, C., Junker, C., Wagner, T., Platt, U., and Jennings, S. G.: The North Atlantic Oscillation controls air pollution transport to the Arctic, Atmos. Chem. Phys., 3, 1769–1778, https://doi.org/10.5194/acp-3-1769-2003, 2003.

Eckhardt, S., Quennehen, B., Olivié, D. J. L., Berntsen, T. K., Cherian, R., Christensen, J. H., Collins, W., Crepinsek, S., Daskalakis, N., Flanner, M., Herber, A., Heyes, C., Hodnebrog, Ø., Huang, L., Kanakidou, M., Klimont, Z., Langner, J., Law, K. S., Lund, M. T., Mahmood, R., Massling, A., Myriokefalitakis, S., Nielsen, I. E., Nøjgaard, J. K., Quaas, J., Quinn, P. K., Raut, J.-C., Rumbold, S. T., Schulz, M., Sharma, S., Skeie, R. B., Skov, H., Uttal, T., von Salzen, K., and Stohl, A.: Current model capabilities for simulating black carbon and sulfate concentrations in the Arctic atmosphere: a multi-model evaluation using a comprehensive measurement data set, Atmos. Chem. Phys., 15, 9413–9433, https://doi.org/10.5194/acp-15-9413-2015, 2015.

Engelmann, R., Ansmann, A., Ohneiser, K., Griesche, H., Radenz, M., Hofer, J., Althausen, D., Dahlke, S., Maturilli, M., Veselovskii, I., Jimenez, C., Wiesen, R., Baars, H., Bühl, J., Gebauer, H., Haarig, M., Seifert, P., Wandinger, U., and Macke, A.: Wildfire smoke, Arctic haze, and aerosol effects on mixed-phase and cirrus clouds over the North Pole region during MOSAiC: an introduction, Atmos. Chem. Phys., 21, 13397–13423, https://doi.org/10.5194/acp-21-13397-2021, 2021.

Engvall, A.-C., Ström, J., Tunved, P., Krejci, R., Schlager, H., and Minikin, A.: The radiative effect of an aged, internally-mixed Arctic aerosol originating from lower-latitude biomass burning, Tellus B, 61, 677–684, 2009.

Evangeliou, N., Balkanski, Y., Hao, W. M., Petkov, A., Silverstein, R. P., Corley, R., Nordgren, B. L., Urbanski, S. P., Eckhardt, S., Stohl, A., Tunved, P., Crepinsek, S., Jefferson, A., Sharma, S., Nøjgaard, J. K., and Skov, H.: Wildfires in northern Eurasia affect the budget of black carbon in the Arctic – a 12-year retrospective synopsis (2002–2013), Atmos. Chem. Phys., 16, 7587–7604, https://doi.org/10.5194/acp-16-7587-2016, 2016.

Fisher, J. A., Jacob, D. J., Purdy, M. T., Kopacz, M., Le Sager, P., Carouge, C., Holmes, C. D., Yantosca, R. M., Batchelor, R. L., Strong, K., Diskin, G. S., Fuelberg, H. E., Holloway, J. S., Hyer, E. J., McMillan, W. W., Warner, J., Streets, D. G., Zhang, Q., Wang, Y., and Wu, S.: Source attribution and interannual variability of Arctic pollution in spring constrained by aircraft (ARCTAS, ARCPAC) and satellite (AIRS) observations of carbon monoxide, Atmos. Chem. Phys., 10, 977–996, https://doi.org/10.5194/acp-10-977-2010, 2010.

Flanner, M. G.: Arctic climate sensitivity to local black carbon, J. Geophys. Res.-Atmos., 118, 1840–1851, https://doi.org/10.1002/jgrd.50176, 2013.

Flanner, M. G., Zender, C. S., Randerson, J. T., and Rasch, P. J.: Present-day climate forcing and response from black carbon in snow, J. Geophys. Res., 112, D11202, https://doi.org/10.1029/2006JD008003, 2007.

Flannigan, M. D. and Harrington, J. B.: A study of the relation of meteorological variables to monthly provincial area burned by wildfire in Canada (1953–1980), J. Appl. Meteorol., 27, 441–452, 1988.

Flemming, J., Benedetti, A., Inness, A., Engelen, R. J., Jones, L., Huijnen, V., Remy, S., Parrington, M., Suttie, M., Bozzo, A., Peuch, V.-H., Akritidis, D., and Katragkou, E.: The CAMS interim Reanalysis of Carbon Monoxide, Ozone and Aerosol for 2003–2015, Atmos. Chem. Phys., 17, 1945–1983, https://doi.org/10.5194/acp-17-1945-2017, 2017.

Fromm, M., Lindsey, D. T., Servranckx, R., Yue, G., Trickl, T., Sica, R., Doucet, P., and Godin-Beekmann, S.: The Untold Story of Pyrocumulonimbus, B. Am. Meteorol. Soc., 91, 1193–1210, https://doi.org/10.1175/2010BAMS3004.1, 2010.

Gabric, A., Matrai, P., Jones, G., and Middleton, J.: The nexus between sea ice and polar emissions of marine biogenic aerosols, B. Am. Meteorol. Soc., 99, 61–81, https://doi.org/10.1175/BAMS-D-16-0254.1, 2018.

Garay, M. J., Witek, M. L., Kahn, R. A., Seidel, F. C., Limbacher, J. A., Bull, M. A., Diner, D. J., Hansen, E. G., Kalashnikova, O. V., Lee, H., Nastan, A. M., and Yu, Y.: Introducing the 4.4 km spatial resolution Multi-Angle Imaging SpectroRadiometer (MISR) aerosol product, Atmos. Meas. Tech., 13, 593–628, https://doi.org/10.5194/amt-13-593-2020, 2020.

Garrett, T. J., Zhao, C., and Novelli, P.: Assessing the relative contributions of transport efficiency and scavenging to seasonal variability in Arctic aerosol, Tellus B, 62, 190–196, https://doi.org/10.1111/j.1600-0889.2010.00453.x, 2010.

Garrett, T. J., Brattström, S., Sharma, S., Worthy, D. E., and Novelli, P.: The role of scavenging in the seasonal transport of black carbon carbon and sulfate to the Arctic, Geophys. Res. Lett., 38, L16805, https://doi.org/10.1029/2011GL048221, 2011.

Giglio, L., Randerson, J. T., and van der Werf, G. R.: Analysis of daily, monthly, and annual burned area using the fourthgeneration global fire emissions database (GFED4), J. Geophys. Res.-Biogeo., 118, 317–328, https://doi.org/10.1002/jgrg.20042, 2013.

Giles, D. M., Sinyuk, A., Sorokin, M. G., Schafer, J. S., Smirnov, A., Slutsker, I., Eck, T. F., Holben, B. N., Lewis, J. R., Campbell, J. R., Welton, E. J., Korkin, S. V., and Lyapustin, A. I.: Advancements in the Aerosol Robotic Network (AERONET) Version 3 database – automated near-real-time quality control algorithm with improved cloud screening for Sun photometer aerosol optical depth (AOD) measurements, Atmos. Meas. Tech., 12, 169–209, https://doi.org/10.5194/amt-12-169-2019, 2019.

Glantz, P., Bourassa, A., Herber A., Iversen T., Karlsson J., Kirkevag, A., Maturilli, M., Seland, O., Stebel, K., Struthers, H., Tesche, M., and Thomason L.: Remote sensing of aerosols in the Arctic for an evaluation of global climate model simulations, J. Geophys. Res. Atmos., 119, 8169–8188, https://doi.org/10.1002/2013JD021279, 2014.

Global Modeling and Assimilation Office (GMAO): MERRA-2 tavgM_2d_aer_Nx: 2d, Monthly mean, Time-averaged, Single-Level, Assimilation, Aerosol Diagnostics V5.12.4, Greenbelt, MD, USA, Goddard Earth Sciences Data and Information Services Center (GES DISC) [data set], https://doi.org/10.5067/FH9A0MLJPC7N, 2015.

Goosse, H., Kay, J. E., Armour, K. C., Bodas-Salcedo, A., Chepfer, H., Docquier, D., Jonko, A., Jusher, P. J., Lecomete, O., Massonnet, F. Park, H., Pithan, F., Svensson, G., and Vancoppenolle, M.: Quantifying climate feedbacks in polar regions, Nat. Commun., 9, 1919, https://doi.org/10.1038/s41467-018-04173-0, 2018.

Graham, R. M., Cohen, L., Petty, A. A., Boisvert, L. N., Rinke, A., Hudson, S. R., Nicolaus, M., and Granskog, M. A.: Increasing frequency and duration of Arctic winter warming events, Geophys. Res. Lett., 44, 6974–6983, https://doi.org/10.1002/2017gl073395, 2017.

Groot Zwaaftink, C. D., Grythe, H., Skov, H., and Stohl, A.: Substantial contribution of northern high-latitude sources to mineral dust in the Arctic, J. Geophys. Res.-Atmos., 121, 13678–13697, https://doi.org/10.1002/2016JD025482, 2016.

Hall, J. V., Loboda, T. V., Giglio, L., and McCarty G. W.: A MODIS-based burned area assessment for Russian croplands: Mapping requirements and challenges, Remote Sens. Environ., 184, 506–521, https://doi.org/10.1016/j.rse.2016.07.022, 2016.

Hansen, J. and Nazarenko, L.: Soot climate forcing via snow and ice albedos, P. Natl. Acad. Sci. USA, 101, 423–428, 2004.

Hansen, E., Gerland, S., Granskog, M. A., Pavlova, O., Renner, A. H. H., Haapala, J., Loyning, T. B., and Tschudi, M.: Thinning of Arctic sea ice observed on Fram Strait: 1990–2011, J. Geophys. Res.-Oceans, 118, 5202–5221, https://doi.org/10.1002/jgrc.20393, 2013.

Heald, C. L., Jacob, D. J., Palmer, P. I., Evans, M. J., Sachse, G. W., Singh, H. B., and Blake, D. R.: Biomass burning emission inventory with daily resolution: Application to aircraft observations of Asian outflow, J. Geophys. Res., 108, 8811, https://doi.org/10.1029/2002JD003082, 2003.

Hegg, D. A., Warren, S. G., Grenfell, T. C., Doherty, S. J., Larson, T. V., and Clarke, A. D.: Source attribution of black carbon in arctic snow, Environ. Sci. Technol., 43, 4016–4021, https://doi.org/10.1021/es803623f, 2009.

Hegg, D. A., Warren, S. G., Grenfell, T. C., Sarah J Doherty, and Clarke, A. D.: Sources of light-absorbing aerosol in arctic snow and their seasonal variation, Atmos. Chem. Phys., 10, 10923–10938, https://doi.org/10.5194/acp-10-10923-2010, 2010.

Herber, A., Thomason, L. W., Gernandt, H., Leiterer, U., Nagel, D., Schulz, K., Kaptur, J., Albrecht, T., and Notholt, J.: Continuous day and night aerosol optical depth observations in the Arctic between 1991 and 1999, J. Geophys. Res., 107, 4097, https://doi.org/10.1029/2001JD000536, 2002.

Hesaraki, S, O'Neill, N.T., Lesins, G., Saha, A., Martin, R. V., Fioletov, V.E., Baibakov, K., and Abboud, I.: Comparisons of a chemical transport model with a four-year (April to September) analysis of fine-and coarse-mode aerosol optical depth retrievals over the Canadian Arctic, Atmosphere-Ocean, 55, 213–229, https://doi.org/10.1080/07055900.2017.1356263, 2017.

Holben, B. N., Eck, T. F., Slutsker, I., Tanre, D., Buis, J. P., Setzer, A., Vermote, E., Reagan, J. A., Kaufman, Y. J., Nakajima, T., Lavenu, F., Jankowiak, I., and Smirnov, A.: AERONET – A federated instrument network and data archive for aerosol characterization, Remote Sens. Environ., 66, 1–16, 1998.

Holben, B. N., Tanré, D., Smirnov, A., Eck, T. F., Slutsker, I.,Abuhassan, N., Newcomb, W. W., Schafer, J. S., Chatenet, B., Lavenu, F., Kaufman, Y. J., Castle, J. V., Setzer, A., Markham, B., Clark, D., Frouin, R., Halthore, R., Karneli, A., O'Neill, N. T., Pietras, C., Pinker, R. T., Voss, K., and Zibordi, G.: An emerging ground-based aerosol climatology: Aerosol optical depth from AERONET, J. Geophys. Res.-Atmos., 106, 12067–12097, 2001.

Hyer, E. J., Reid, J. S., and Zhang, J.: An over-land aerosol optical depth data set for data assimilation by filtering, correction, and aggregation of MODIS Collection 5 optical depth retrievals, Atmos. Meas. Tech., 4, 379–408, https://doi.org/10.5194/amt-4-379-2011, 2011.

Hyer, E. J., Reid, J. S., Prins, E. M., Hoffman, J. P., Schmidt, C. C., Miettinen, J. I., and Giglio, L.: Patterns of fire activity over Indonesia and Malaysia from polar and geostationary satellite observations, Atmos. Res., 122, 504–519, https://doi.org/10.1016/J.Atmosres.2012.06.011, 2013.

Inness, A., Baier, F., Benedetti, A., Bouarar, I., Chabrillat, S., Clark, H., Clerbaux, C., Coheur, P., Engelen, R. J., Errera, Q., Flemming, J., George, M., Granier, C., Hadji-Lazaro, J., Huijnen, V., Hurtmans, D., Jones, L., Kaiser, J. W., Kapsomenakis, J., Lefever, K., Leitão, J., Razinger, M., Richter, A., Schultz, M. G., Simmons, A. J., Suttie, M., Stein, O., Thépaut, J.-N., Thouret, V., Vrekoussis, M., Zerefos, C., and the MACC team: The MACC reanalysis: an 8 yr data set of atmospheric composition, Atmos. Chem. Phys., 13, 4073–4109, https://doi.org/10.5194/acp-13-4073-2013, 2013.

Inness, A., Ades, M., Agustí-Panareda, A., Barré, J., Benedictow, A., Blechschmidt, A.-M., Dominguez, J. J., Engelen, R., Eskes, H., Flemming, J., Huijnen, V., Jones, L., Kipling, Z., Massart, S., Parrington, M., Peuch, V.-H., Razinger, M., Remy, S., Schulz, M., and Suttie, M.: The CAMS reanalysis of atmospheric composition, Atmos. Chem. Phys., 19, 3515–3556, https://doi.org/10.5194/acp-19-3515-2019, 2019.

IPCC: Climate change 2021: The physical science basis, Chapter 6, Short-Lived Climate Forcers, edited by: Masson-Delmotte,V., Zhai, P., Pirani, A., Connors, S. L., Péan, C., Berger, S.,Caud, N., Chen, Y., Goldfarb, L., Gomis, M. I., Huang, M., Leitzell, K., Lonnoy, E., Matthews, J. B. R., Maycock, T., K., Waterfield, T., Yelekci, O., Yu, R., and Zhou, B., Cambridge University Press, Cambridge, United Kingdom and New York, NY, USA, 817–922, https://doi.org/10.1017/9781009157896.008, 2021a.

IPCC: Climate change 2021: The physical science basis, Chapter 7: The Earth's Energy Budget, Climate Feedbacks, and Climate Sensitivity, edited by: Masson-Delmotte, V., Zhai, P., Pirani, A., Connors, S. L., Péan, C., Berger, S.,Caud, N., Chen, Y., Goldfarb, L., Gomis, M. I., Huang, M., Leitzell, K., Lonnoy, E., Matthews, J. B. R., Maycock, T., K., Waterfield, T., Yelekci, O., Yu, R., and Zhou, B., Cambridge University Press, Cambridge, United Kingdom and New York, NY, USA, 923–1054, https://doi.org/10.1017/9781009157896.009, 2021b.

Iziomon, M. G., Lohmann, U., and Quinn, P. K.: Summertime pollution events in the Arctic and potential implications, J. Geophys. Res., 111, D12206, https://doi.org/10.1029/2005JD006223, 2006.

Jacob, D. J., Crawford, J. H., Maring, H., Clarke, A. D., Dibb, J. E., Emmons, L. K., Ferrare, R. A., Hostetler, C. A., Russell, P.

B., Singh, H. B., Thompson, A. M., Shaw, G. E., McCauley, E., Pederson, J. R., and Fisher, J. A.: The Arctic Research of the Composition of the Troposphere from Aircraft and Satellites (ARCTAS) mission: design, execution, and first results, Atmos. Chem. Phys., 10, 5191–5212, https://doi.org/10.5194/acp-10-5191-2010, 2010.

Jacobson, M. Z.: Climate response of fossil fuel and biofuel soot, accounting for soot's feedback to snow and sea ice albedo and emissivity, J. Geophys. Res., 109, D21201, https://doi.org/10.1029/2004JD004945, 2004.

Kaku, K. C., Reid, J. S., O'Neill, N. T., Quinn, P. K., Coffman, D. J., and Eck, T. F.: Verification and application of the extended spectral deconvolution algorithm (SDA+) methodology to estimate aerosol fine and coarse mode extinction coefficients in the marine boundary layer, Atmos. Meas. Tech., 7, 3399–3412, https://doi.org/10.5194/amt-7-3399-2014, 2014.

Kang S., Zhang, Y., Qian, Y., and Wang, Y.: A review of black carbon in snow and ice and its impact on the cryosphere, Earth Sci. Rev., 210, PNNL-SA-154137, https://doi.org/10.1016/j.earscirev.2020.103346, 2020.

Kapsch, M.-L., Graversen, R. G., and Tjernström, M.: Springtime atmospheric energy transport and the control of Arctic summer sea-ice extent, Nat. Clim. Change, 3, 744, https://doi.org/10.1038/nclimate1884, 2013.

Kahn, R. A., Gaitley, B. J., Garay, M. J., Diner, D. J., Eck, T. F., Smirnov, A. and Holben, B. N.: Multiangle Imaging SpectroRadiometer global aerosol product assessment by comparison with the Aerosol Robotic Network, J. Geophys. Res., 115, D23209, https://doi.org/10.1029/2010JD014601, 2010.

Kaiser, J. W., Heil, A., Andreae, M. O., Benedetti, A., Chubarova, N., Jones, L., Morcrette, J.-J., Razinger, M., Schultz, M. G., Suttie, M., and van der Werf, G. R.: Biomass burning emissions estimated with a global fire assimilation system based on observed fire radiative power, Biogeosciences, 9, 527–554, https://doi.org/10.5194/bg-9-527-2012, 2012.

Khan, A. L., Wagner, S., Jaffe, R., Xian, P., Williams, M., Armstrong, R., and McKnight, D.: Dissolved black carbon in the global cryosphere: Concentrations and chemical signatures, Geophys. Res. Lett., 44, 6226–6234, https://doi.org/10.1002/2017GL073485, 2017.

Kim, J. S., Kug, J. S., Jeong, S. J., Park, H., and Schaepman-Strub, G.: Extensive fires in southeastern Siberian permafrost linked to preceding Arctic Oscillation, Sci. Adv., 6, eaax3308, https://doi.org/10.1126/sciadv.aax3308, 2020.

Kim, M.-H., Omar, A. H., Tackett, J. L., Vaughan, M. A., Winker, D. M., Trepte, C. R., Hu, Y., Liu, Z., Poole, L. R., Pitts, M. C., Kar, J., and Magill, B. E.: The CALIPSO version 4 automated aerosol classification and lidar ratio selection algorithm, Atmos. Meas. Tech., 11, 6107–6135, https://doi.org/10.5194/amt-11-6107-2018, 2018.

Kleidman, R. G., O'Neill, N., T., Remer, L. A., Kaufman, Y. J., Eck, T. F., Tanré, D., Dubovik, O., and Holben, B. N.: Comparison of Moderate Resolution Imaging Spectroradiometer (MODIS) and Aerosol Robotic Network (AERONET) remote-sensing retrievals of aerosol fine mode fraction over ocean, J. Geophys. Res., 110, D22205, https://doi.org/10.1029/2005JD005760, 2005.

Kokhanovsky, A. and Tomasi, C. (Eds.): Physics and Chemistry of the Arctic Atmosphere, Springer Nature Switzerland AG, https://doi.org/10.1007/978-3-030-33566-3, 2020.

Kondo, Y., Matsui, H., Moteki, N., Sahu, L., Takegawa, N., Kajino, M., Zhao, Y., Cubison, M. J., Jimenez, J. L., Vay, S., Diskin, G. S., Anderson, B., Wisthaler, A., Mikoviny, T., Fuelberg, H. E., Blake, D. R., Huey, G., Weinheimer, A. J., Knapp, D. J., and Brune, W. H.: Emissions of black carbon, organic, and inorganic aerosols from biomass burning in North America and Asia in 2008, J. Geophys. Res., 116, D08204, https://doi.org/10.1029/2010JD015152, 2011.

Korontzi, S., McCarty, J., Loboda, T., Kumar, S., and Justice, C.: Global distribution of agricultural fires in croplands from 3 years of Moderate Resolution Imaging Spectroradiometer (MODIS) data, Global Biogeochem. Cycles, 20, GB2021, https://doi.org/10.1029/2005GB002529, 2006.

Kwok, R. and Rothrock D. A.: Decline in Arctic sea ice thickness from submarine and ICESate records: 1958–2008, Geophys. Res. Lett., 36, L15501, https://doi.org/10.1029/2009GL039035, 2009.

Lance, S., Shupe, M. D., Feingold, G., Brock, C. A., Cozic, J., Holloway, J. S., Moore, R. H., Nenes, A., Schwarz, J. P., Spackman, J. R., Froyd, K. D., Murphy, D. M., Brioude, J., Cooper, O. R., Stohl, A., and Burkhart, J. F.: Cloud condensation nuclei as a modulator of ice processes in Arctic mixed-phase clouds, Atmos. Chem. Phys., 11, 8003–8015, https://doi.org/10.5194/acp-11-8003-2011, 2011.

Law, K. S. and Stohl, A.: Arctic air pollution: Origins and impacts, Science, 315, 1537–1540, https://doi.org/10.1126/science.1137695, 2007.

Levy, R. C., Mattoo, S., Munchak, L. A., Remer, L. A., Sayer, A. M., Patadia, F., and Hsu, N. C.: The Collection 6 MODIS aerosol products over land and ocean, Atmos. Meas. Tech., 6, 2989–3034, https://doi.org/10.5194/amt-6-2989-2013, 2013.

Lubin, D. and Vogelmann, A. M.: A climatologically significant aerosol longwave indirect effect in the Arctic, Nature, 439, 453–456, https://doi.org/10.1038/nature04449, 2006.

Lynch, P., Reid, J. S., Westphal, D. L., Zhang, J., Hogan, T. F., Hyer, E. J., Curtis, C. A., Hegg, D. A., Shi, Y., Campbell, J. R., Rubin, J. I., Sessions, W. R., Turk, F. J., and Walker, A. L.: An 11-year global gridded aerosol optical thickness reanalysis (v1.0) for atmospheric and climate sciences, Geosci. Model Dev., 9, 1489–1522, https://doi.org/10.5194/gmd-9-1489-2016, 2016.

Macias Fauria, M. and Johnson, E. A.: Large-scale climatic patterns control large lightning fire occurrence in Canada and Alaska forest regions, J. Geophys. Res., 111, G04008, https://doi.org/10.1029/2006JG000181, 2006.

Markowicz, K. M., Pakszys, R., Ritter, C., Zielensi, T., Udisti, R., Cappelletti, D., Mazzola, M., Shobara, M., Xian, P., Zawadzka, O., Lisok, J., Petelski, T., Makuch, P., and Karasinksi, G.: Impact of North American intense fires on aerosol optical properties measured over the European Arctic in July 2015, J. Geophys. Res.-Atmos., 121, 14487–14512, https://doi.org/10.1002/2016JD025310, 2016.

Markowicz, K. M., Lisok, J., and Xian, P.: Simulation of long-term direct aerosol radiative forcing over the arctic within the framework of the iAREA project, Atmos. Environ., 244, 117882, https://doi.org/10.1016/j.atmosenv.2020.117882, 2021.

Matsui, H., Kondo, Y., Moteki, N., Takegawa, N., Sahu, L. K., Zhao, Y., Fuelberg, H. E., Sessions, W. R., Diskin, G., Blake, D. R.,

Wisthaler, A., and Koike, M.: Seasonal variation of the transport of black carbon aerosol from the Asian continent to the Arctic during the ARCTAS aircraft campaign, J. Geophys. Res.-Atmos., 116, D05202, https://doi.org/10.1029/2010JD015067, 2011.

Mauritsen, T., Sedlar, J., Tjernström, M., Leck, C., Martin, M., Shupe, M., Sjogren, S., Sierau, B., Persson, P. O. G., Brooks, I. M., and Swietlicki, E.: An Arctic CCN-limited cloud-aerosol regime, Atmos. Chem. Phys., 11, 165–173, https://doi.org/10.5194/acp-11-165-2011, 2011.

McCarty, J. L., Aalto, J., Paunu, V.-V., Arnold, S. R., Eckhardt, S., Klimont, Z., Fain, J. J., Evangeliou, N., Venäläinen, A., Tchebakova, N. M., Parfenova, E. I., Kupiainen, K., Soja, A. J., Huang, L., and Wilson, S.: Reviews and syntheses: Arctic fire regimes and emissions in the 21st century, Biogeosciences, 18, 5053–5083, https://doi.org/10.5194/bg-18-5053-2021, 2021.

McNaughton, C. S., Clarke, A. D., Freitag, S., Kapustin, V. N., Kondo, Y., Moteki, N., Sahu, L., Takegawa, N., Schwarz, J. P., Spackman, J. R., Watts, L., Diskin, G., Podolske, J., Holloway, J. S., Wisthaler, A., Mikoviny, T., de Gouw, J., Warneke, C., Jimenez, J., Cubison, M., Howell, S. G., Middlebrook, A., Bahreini, R., Anderson, B. E., Winstead, E., Thornhill, K. L., Lack, D., Cozic, J., and Brock, C. A.: Absorbing aerosol in the troposphere of the Western Arctic during the 2008 ARCTAS/AR-CPAC airborne field campaigns, Atmos. Chem. Phys., 11, 7561–7582, https://doi.org/10.5194/acp-11-7561-2011, 2011.

Meier, W. N., Hovelsrud, G. K., van Oort, B. E., Key, J. R., Kovacs, K. M., Michel, C., Haas, C., Granskog, M. A., Gerland, S., Perovich, D. K., Makshtas, A., and Reist, J. D.: Arctic sea ice in transformation: A review of recent observed changes and impacts on biology and human activity, Rev. Geophys., 52, 185–217, https://doi.org/10.1002/2013RG000431, 2014.

Morrison, A. L., Kay, J. E., Chepfer, H., Guzman, R., and Yettella, V.: Isolating the Liquid Cloud Response to Recent Arctic Sea Ice Variability Using Spaceborne Lidar Observations, J. Geophys. Res.-Atmos., 123, 473–490, https://doi.org/10.1002/2017JD027248, 2018.

NASA: MAN AOD data, NASA [data set], https://aeronet.gsfc.nasa.gov/new_web/maritime_aerosol_network.html, curator David M. Giles, last access: 10 July 2022a.

NASA: Multi-angle Imaging SpectroRadiometer (MISR) Level 2 Aerosol parameters Verion 3, NASA Langley ASDC User Services [data set], https://doi.org/10.5067/TERRA/MISR/MIL2ASAE_L2.003-23, 2022b.

NASA/LARC/SD/ASDC: CALIPSO Lidar Level 2 Aerosol Profile, V4-20, NASA/LARC/SD/ASDC [data set], https://doi.org/10.5067/CALIOP/CALIPSO/LID_L2_05KMAPRO-STANDARD-V4-20, 2018a.

NASA/LARC/SD/ASDC: CALIPSO Lidar Level 2 5 km Aerosol Layer Data, V4-20, NASA/LARC/SD/ASDC [data set], https://doi.org/10.5067/CALIOP/CALIPSO/LID_L2_05KMALAY-STANDARD-V4-20, 2018b.

Notz, D. and Stroeve, J.: Observed Arctic sea-ice loss directly follows anthropogenic CO_2 emission. Science, 354, 747–750, https://doi.org/10.1126/science.aag2345, 2016.

Nummelin, A., Li, C., and Hezel, P. J.: Connecting ocean heat transport changes from the midlatitudes to the Arctic Ocean, Geophys. Res. Lett., 44, 1899–1908, https://doi.org/10.1002/2016GL071333, 2017.

O'Neill, N. T., Eck, T. F., Holben, B. N., Smirnov, A., Dubovik, O., and Royer, A.: Bimodal size distribution influences on the variation of Angstrom derivatives in spectral and optical depth space, J. Geophys. Res., 106, 9787–9806, 2001.

O'Neill, N. T., Eck, T. F., Smirnov, A., Holben, B. N., and Thulasiraman, S.: Spectral discrimination of coarse and fine mode optical depth, J. Geophys. Res., 108, D05212, https://doi.org/10.1029/2002JD002975, 2003.

O'Neill, N. T., Perro, C., Saha, A., Lesins, G., Duck, T. J., Eloranta, E. W., Nott, G. J., Hoffman, A., Karumudi, M. L., Ritter, C., Bourassa, A., Abboud, I., Carn S., A., and Savastiouk, V.: Properties of Sarycheve Sulphate aerosols over the Arctic, J. Geophys. Res.-Atmos., 117, D04203, https://doi.org/10.1029/2011JD016838, 2012.

Perovich, D. K. and Polashenski, C.: Albedo evolution of seasonal Arctic sea ice, Geophys. Res. Lett., 39, L08501, https://doi.org/10.1029/2012GL051432, 2012.

Peterson, D. A., Hyer, E. J., Campbell, J. R., Fromm, M. D., Hair, J. W., Butler, C. F., and Fenn, M. A.: The 2013 Rim Fire: Implications for Predicting Extreme Fire Spread, Pyroconvection, and Smoke Emissions, B. Am. Meteorol. Soc., 96, 229–247, 2015.

Peterson, D. A., Fromm, M. D., Solbrig, J. E., Hyer, E. J., Surratt, M. L., and Campbell, J. R.: Detection and Inventory of Intense Pyroconvection in Western North America using GOES-15 Day-time Infrared Data, J. Appl. Meteorol. Climatol., 56, 471–493, 2017.

Prenni, A. J., Harrington, J. Y., Tjernström, M., DeMott, P. J., Avramov, A., Long, C. N., Kreidenweis, S. M., Olsson, P. Q., and Verlinde, J.: Can ice-nucleating aerosols affect arctic seasonal climate?, B. Am. Meteorol. Soc., 88, 541–550, https://doi.org/10.1175/BAMS-88-4-541, 2007.

Quinn, P. K., Bates, T. S., Baum, E., Doubleday, N., Fiore, A. M., Flanner, M., Fridlind, A., Garrett, T. J., Koch, D., Menon, S., Shindell, D., Stohl, A., and Warren, S. G.: Short-lived pollutants in the Arctic: their climate impact and possible mitigation strategies, Atmos. Chem. Phys., 8, 1723–1735, https://doi.org/10.5194/acp-8-1723-2008, 2008.

Randerson, J. T., Liu, H., Flanner, M. G., Chambers, S. D., Jin, Y., Hess, P. G., Pfister, G., Mack, M. C., Treseder, K. K., Welp, L. R., Chapin, F. S., Harden, J. W., Goulden, M. L., Lyons, E., Neff, J. C., Schuur, E. A. G., and Zender, C. S.: The impact of boreal forest fire on climate warming, Science, 314, 1130–1132, https://doi.org/10.1126/science.1132075, 2006.

Randles, C. A., daSilva, A. M., Buchard, V., Colarco, P. R., Darmenov, A., Govindaraju, R., Smirnov, A., Holben, B., Ferrare, R., Hair, J., Shinozuka, Y., and Flynn, C. J.: The MERRA-2 aerosol reanalysis, 1980 onward. Part I: System description and data assimilation evaluation, J. Climate, 30, 6823–6850, https://doi.org/10.1175/JCLI-D-16-0609.1, 2017.

Ranjbar, K., O'Neill, N. T., Lutsch, E., McCullough, E. M., AboEl-Fetouh, Y., Xian, P., Strong, K., Fioletov, V. E., Sesins, G., and Abboud, I.: Extreme smoke event over the high Arctic, Atmos. Environ., 218, 117002, https://doi.org/10.1016/j.atmosenv.2019.117002, 2019.

Reid, J. S., Hyer, E. J., Prins, E. M., Westphal, D. L., Zhang, J., Wang, J., Christopher, S. A., Curtis, C. A., Schmidt, C. C., Eleuterio, D. P., Richardson, K. A., and Hoffman, J. P.: Global Monitoring and Forecasting of Biomass-Burning Smoke: Description of and Lessons from the Fire Locating and Modeling of Burn-

ing Emissions (FLAMBE) Program, IEEE J. Sel. Top. Appl., 2, 144–162, 2009.

Ren, L., Yang, Y., Wang, H., Zhang, R., Wang, P., and Liao, H.: Source attribution of Arctic black carbon and sulfate aerosols and associated Arctic surface warming during 1980–2018, Atmos. Chem. Phys., 20, 9067–9085, https://doi.org/10.5194/acp-20-9067-2020, 2020.

Rinke, A., Maturilli, M., Graham, R. M., Matthes, H., Handorf, D., Cohen, L., Hudson, S. R., and Moore, J. C.: Extreme cyclone events in the Arctic: Wintertime variability and trends, Environ. Res. Lett., 12, 094006, https://doi.org/10.1088/1748-9326/aa7def, 2017.

Rosel, A., Itkin, P., King, J., Divine, D., Wang, C., Granskog, M. A., Krumpen, T., and Gerland, S.: Thin sea ice, thick snow and widespread negative freeboard observed during N-ICE2015 north of Svalbard, J. Geophys. Res.-Oceans, 123, 1156–1176, https://doi.org/10.1002/2017JC012865, 2018.

Saha, A., O'Neill, N. T., Eloranta, E., Stone, R. S., Eck, T. F., Zidane, S., Daou, D., Lupu, A., Lesins, G., and Shiobara, M.: Pan-Arctic sunphotometry during the ARCTAS-A campaign of April 2008, Geophys. Res. Lett., 37, L05803, https://doi.org/10.1029/2009GL041375, 2010.

Sand, M., Berntsen, T. K., Seland, Ø., and Kristjánsson, J. E.: Arctic surface temperature change to emissions of black carbon within Arctic or midlatitudes, J. Geophys. Res.-Atmos., 118, 7788–7798, https://doi.org/10.1002/jgrd.50613, 2013.

Sand, M., Berntsen, T., Von Salzen, K., Flanner, M., Langner, J., and Victor, D.: Response of Arctic temperature to changes in emissions of short-lived climate forcers, Nat. Clim. Change, 6, 286–289, https://doi.org/10.1038/nclimate2880, 2016.

Sand, M., Samset, B. H., Balkanski, Y., Bauer, S., Bellouin, N., Berntsen, T. K., Bian, H., Chin, M., Diehl, T., Easter, R., Ghan, S. J., Iversen, T., Kirkevåg, A., Lamarque, J.-F., Lin, G., Liu, X., Luo, G., Myhre, G., Noije, T. V., Penner, J. E., Schulz, M., Seland, Ø., Skeie, R. B., Stier, P., Takemura, T., Tsigaridis, K., Yu, F., Zhang, K., and Zhang, H.: Aerosols at the poles: an AeroCom Phase II multi-model evaluation, Atmos. Chem. Phys., 17, 12197–12218, https://doi.org/10.5194/acp-17-12197-2017, 2017.

Sayer, A. M. and Knobelspiesse, K. D.: How should we aggregate data? Methods accounting for the numerical distributions, with an assessment of aerosol optical depth, Atmos. Chem. Phys., 19, 15023–15048, https://doi.org/10.5194/acp-19-15023-2019, 2019.

Schmale, J., Zieger, P., and Ekman, A. M. L.: Aerosols in current and future Arctic climate, Nat. Clim. Chang., 11, 95–105, https://doi.org/10.1038/s41558-020-00969-5, 2021.

Schmale, J., Sharma, S., Decesari, S., Pernov, J., Massling, A., Hansson, H.-C., von Salzen, K., Skov, H., Andrews, E., Quinn, P. K., Upchurch, L. M., Eleftheriadis, K., Traversi, R., Gilardoni, S., Mazzola, M., Laing, J., and Hopke, P.: Pan-Arctic seasonal cycles and long-term trends of aerosol properties from 10 observatories, Atmos. Chem. Phys., 22, 3067–3096, https://doi.org/10.5194/acp-22-3067-2022, 2022.

Serreze, M. C. and Barry, R. G.: Processes and impacts of Arctic amplification: A research synthesis, Global Planet. Change, 77, 85–96, https://doi.org/10.1016/j.gloplacha.2011.03.004, 2011.

Serreze, M. C. and Francis, J. A.: The Arctic Amplification Debate, Clim. Change, 76, 241–264, https://doi.org/10.1007/s10584-005-9017-y, 2006.

Sessions, W. R., Reid, J. S., Benedetti, A., Colarco, P. R., da Silva, A., Lu, S., Sekiyama, T., Tanaka, T. Y., Baldasano, J. M., Basart, S., Brooks, M. E., Eck, T. F., Iredell, M., Hansen, J. A., Jorba, O. C., Juang, H.-M. H., Lynch, P., Morcrette, J.-J., Moorthi, S., Mulcahy, J., Pradhan, Y., Razinger, M., Sampson, C. B., Wang, J., and Westphal, D. L.: Development towards a global operational aerosol consensus: basic climatological characteristics of the International Cooperative for Aerosol Prediction Multi-Model Ensemble (ICAP-MME), Atmos. Chem. Phys., 15, 335–362, https://doi.org/10.5194/acp-15-335-2015, 2015.

Shi, Y., Zhang, J., Reid, J. S., Holben, B., Hyer, E. J., and Curtis, C.: An analysis of the collection 5 MODIS over-ocean aerosol optical depth product for its implication in aerosol assimilation, Atmos. Chem. Phys., 11, 557–565, https://doi.org/10.5194/acp-11-557-2011, 2011.

Shi, Y., Zhang, J., Reid, J. S., Hyer, E. J., and Hsu, N. C.: Critical evaluation of the MODIS Deep Blue aerosol optical depth product for data assimilation over North Africa, Atmos. Meas. Tech., 6, 949–969, https://doi.org/10.5194/amt-6-949-2013, 2013.

Shindell, D. and Faluvegi, G.: Climate response to regional radiative forcing during the twentieth century, Nat. Geosci., 2, 294–300, https://doi.org/10.1038/ngeo473, 2009.

Skiles, S. M., Flanner, M., Cook, J. M., Dumont, M., and Painter, T.: Radiative forcing by light-absorbing particles in snow, Nat. Clim. Change, 8, 964–971, https://doi.org/10.1038/s41558-018-0296-5, 2018.

Skinner, W. R., Stocks, B. J., Martell, D. L., Bonsal, B., and Shabbar, A.: The association between circulation anomalies in the mid-troposphere and area burned by wildland fire in Canada, Theor. Appl. Climatol., 63, 89–105, 1999.

Smirnov, A., Holben, B. N., Slutsker, I., Giles, D. M., McClain, C. R., Eck, T. F., Sakerin, S. M., Macke, A., Croot, P., Zibordi, G., Quinn, P. K., Sciare, J., Kinne, S., Harvey, M., Smyth, T. J., Piketh, S., Zielinski, T., Proshutinsky, A., Goes, J. I., Nelson, N. B., Larouche, P., Radionov, V. F., Goloub, P., Krishna Moorthy, K., Matarrese, R., Robertson, E. J., and Jourdin, F.: Maritime Aerosol Network as a component of Aerosol Robotic Network, J. Geophys. Res.-Atmos., 114, D06204, https://doi.org/10.1029/2008JD011257, 2009.

Smirnov, A., Holben, B. N., Giles, D. M., Slutsker, I., O'Neill, N. T., Eck, T. F., Macke, A., Croot, P., Courcoux, Y., Sakerin, S. M., Smyth, T. J., Zielinski, T., Zibordi, G., Goes, J. I., Harvey, M. J., Quinn, P. K., Nelson, N. B., Radionov, V. F., Duarte, C. M., Losno, R., Sciare, J., Voss, K. J., Kinne, S., Nalli, N. R., Joseph, E., Krishna Moorthy, K., Covert, D. S., Gulev, S. K., Milinevsky, G., Larouche, P., Belanger, S., Horne, E., Chin, M., Remer, L. A., Kahn, R. A., Reid, J. S., Schulz, M., Heald, C. L., Zhang, J., Lapina, K., Kleidman, R. G., Griesfeller, J., Gaitley, B. J., Tan, Q., and Diehl, T. L.: Maritime aerosol network as a component of AERONET – first results and comparison with global aerosol models and satellite retrievals, Atmos. Meas. Tech., 4, 583–597, https://doi.org/10.5194/amt-4-583-2011, 2011.

Stohl, A., Andrews, E., Burkhart, J. F., Forster, C., Herber, A., Hoch, S. W., Kowal, D., Lunder, C., Mefford, T., Ogren, J. A., Sharma, S., Spichtinger, N., Stebel, K., Stone, R., Strom, J., Torseth, K., Wehrli, C., and Yttri, K. E.: Pan-Arctic enhancements of light

absorbing aerosol concentrations due to North American boreal forest fires during summer 2004, J. Geophys. Res.-Atmos., 111, D22214, https://doi.org/10.1029/2006jd007216, 2006.

Stohl, A., Berg, T., Burkhart, J. F., Fjǽraa, A. M., Forster, C., Herber, A., Hov, Ø., Lunder, C., McMillan, W. W., Oltmans, S., Shiobara, M., Simpson, D., Solberg, S., Stebel, K., Ström, J., Tørseth, K., Treffeisen, R., Virkkunen, K., and Yttri, K. E.: Arctic smoke – record high air pollution levels in the European Arctic due to agricultural fires in Eastern Europe in spring 2006, Atmos. Chem. Phys., 7, 511–534, https://doi.org/10.5194/acp-7-511-2007, 2007.

Stone, R. S., Anderson, G. P., Andrews, E., Dutton, E. G., Shettle, E. P., and Berk, A.: Incursions and radiative impact of Asian dust in northern Alaska, Geophys. Res. Lett., 34, L14815, https://doi.org/10.1029/2007GL029878, 2007.

Taylor, P., Hegyi, B., Boeke, R., and Boisvert, L.: On the Increasing Importance of Air-Sea Exchanges in a Thawing Arctic: A Review, Atmosphere, 9, 41, https://doi.org/10.3390/atmos9020041, 2018.

The Naval Research Laboratory and the University of North Dakota/MODIS Adaptive Processing System (MODAPS): Terra Product Descriptions: MCDAODHD, NASA [data set], https://doi.org/10.5067/MODIS/MCDAODHD.NRT.061, 2017.

Thomason, L. W., Ernest, N., Millán, L., Rieger, L., Bourassa, A., Vernier, J.-P., Manney, G., Luo, B., Arfeuille, F., and Peter, T.: A global space-based stratospheric aerosol climatology: 1979–2016, Earth Syst. Sci. Data, 10, 469–492, https://doi.org/10.5194/essd-10-469-2018, 2018.

Tomasi, C., Vitale, V., Lupi, A., Di Carmine, C., Campanelli, M., Herber, A., Treffeisen, R., Stone, R. S., Andrews, E., Sharma, S., Radionov, V., von Hoyningen-Huene, W., Stebel, K., Hansen, G. H., Myhre, C. L.,Wehrli, C., Aaltonen, V., Lihavainen, H., Virkkula, A., Hillamo, R., Ström, J., Toledano, C., Cachorro, V. E., Ortiz, P., de Frutos, A. M., Blindheim, S., Frioud, M., Gausa, M., Zielinski, T., Petelski, T., and Yamanouchi, T.: Aerosols in polar regions: a historical overview based on optical depth and in situ observations, J. Geophys. Res.-Atmos., 112, D16, https://doi.org/10.1029/2007JD008432, 2007.

Tomasi, C., Kokhanovsky, A. A., Lupi, A., Ritter, C., Smirnov, A., O'Neill, N. T., Stone, R. S., Holben, B. N., Nyeki, S., Wehrli, C., Stohl, A., Mazzola, M., Lanconelli, C., Vitale, V., Stebel, K., Aaltonen, V., de Leeuw, G., Rodriguez, E., Herber, A. B., Radionov, V. F., Zielinski, T., Petelski, T., Sakerin, S. M., Kabanov, D. M., Xue, Y., Mei, L., Istomina, L., Wagener, R., McArthur, B., Sobolewski, P. S., Kivi, R., Courcoux, Y., Larouche, P., Broccardo, S., and Piketh, S. J.: Aerosol remote sensing in polar regions, Earth-Sci. Rev., 140, 108–157, https://doi.org/10.1016/j.earscirev.2014.11.001, 2015.

Toth, T. D., Zhang, J., Campbell, J. R., Reid, J. S., and Vaughan, M. A.: Temporal variability of aerosol optical thickness vertical distribution observed from CALIOP, J. Geophys. Res.-Atmos., 121, 9117–9139, 2016.

Toth, T. D., Campbell, J. R., Reid, J. S., Tackett, J. L., Vaughan, M. A., Zhang, J., and Marquis, J. W.: Minimum aerosol layer detection sensitivities and their subsequent impacts on aerosol optical thickness retrievals in CALIPSO level 2 data products, Atmos. Meas. Tech., 11, 499–514, https://doi.org/10.5194/amt-11-499-2018, 2018.

Valkonen, E., Cassano, J., and Cassano, E.: Arctic cyclones and their interactions with the declining sea ice: A recent climatology, J. Geophys. Res.-Atmos., 126, e2020JD034366, https://doi.org/10.1029/2020JD034366, 2021.

Val Martin, M., Logan, J. A., Kahn, R. A., Leung, F.-Y., Nelson, D. L., and Diner, D. J.: Smoke injection heights from fires in North America: analysis of 5 years of satellite observations, Atmos. Chem. Phys., 10, 1491–1510, https://doi.org/10.5194/acp-10-1491-2010, 2010.

van der Werf, G. R., Randerson, J. T., Giglio, L., Collatz, G. J., Kasibhatla, P. S., and Arellano Jr., A. F.: Interannual variability in global biomass burning emissions from 1997 to 2004, Atmos. Chem. Phys., 6, 3423–3441, https://doi.org/10.5194/acp-6-3423-2006, 2006.

Wang, Y., Jiang, J. H., Su, H., Choi, S., Huang, L., Guo, J., and Yung, Y.: Elucidating the Role of Anthropogenic Aerosols In Arctic Sea Ice Variations, J. Climate, 31, 99–114, 2018.

Warneke, C., Froyd, K., Brioude, J., Bahreini, R., Brock, C., Cozic, J., De Gouw, J., Fahey, D., Ferrare, R., and Holloway, J.: An important contribution to springtime Arctic aerosol from biomass burning in Russia, Geophys. Res. Lett., 37, L01801, https://doi.org/10.1029/2009GL041816, 2010.

Waseda, T., Nose, T., Kodaira, T, Sasmal, K and Webb, A.: Climatic trends of extreme wave events caused by Arctic cyclones in the western Arctic Ocean, Polar Sci., 27, 100625, https://doi.org/10.1016/j.polar.2020.100625, 2021.

Weatherhead, E. C., Reinsel, G. C., Tiao, G. C., Meng, X.-L., Choi, D., Cheang, W.-K., Keller, T., DeLuisi, J., Wuebbles, D. J., Kerr, J. B., Miller, A. J., Oltmans, S. J., and Frederick, J. E.: Factors affecting the detection of trends: Statistical considerations and applications to environmental data, J. Geophys. Res., 103, 17149–17161, https://doi.org/10.1029/98JD00995, 1998.

Wendisch, M., Macke, A., Ehrlich, A., Lüpkes, C., Mech, M., Chechin, D., Dethloff, K., Velasco, C. B., Bozem, H., Brückner, M., Clemen, H.-C., Crewell, S., Donth, T., Dupuy, R., Ebell, K., Egerer, U., Engelmann, R., Engler, C., Eppers, O., Gehrmann, M., Gong, X., Gottschalk, M., Gourbeyre, C., Griesche, H., Hartmann, J., Hartmann, M., Heinold, B., Herber, A., Herrmann, H., Heygster, G., Hoor, P., Jafariserajehlou, S., Jäkel, E., Järvinen, E., Jourdan, O., Kästner, U., Kecorius, S., Knudsen, E. M., Köllner, F., Kretzschmar, J., Lelli, L., Leroy, D., Maturilli, M., Mei, L., Mertes, S., Mioche, G., Neuber, R., Nicolaus, M., Nomokonova, T., Notholt, J., Palm, M., van Pinxteren, M., Quaas, J., Richter, P., Ruiz-Donoso, E., Schäfer, M., Schmieder, K., Schnaiter, M., Schneider, J., Schwarzenböck, A., Seifert, P., Shupe, M. D., Siebert, H., Spreen, G., Stapf, J., Stratmann, F., Vogl, T., Welti, A., Wex, H., Wiedensohler, A., Zanatta, M., and Zeppenfeld, S.: The Arctic Cloud Puzzle: Using ACLOUD/PASCAL Multiplatform Observations to Unravel the Role of Clouds and Aerosol Particles in Arctic Amplification, B. Am. Meteorol. Soc., 100, 841–871, https://doi.org/10.1175/BAMS-D-18-0072.1, 2019.

Wex, H., Huang, L., Zhang, W., Hung, H., Traversi, R., Becagli, S., Sheesley, R. J., Moffett, C. E., Barrett, T. E., Bossi, R., Skov, H., Hünerbein, A., Lubitz, J., Löffler, M., Linke, O., Hartmann, M., Herenz, P., and Stratmann, F.: Annual variability of ice-nucleating particle concentrations at different Arctic locations, Atmos. Chem. Phys., 19, 5293–5311, https://doi.org/10.5194/acp-19-5293-2019, 2019.

Winker, D. M., Pelon, J. R., and McCormick, M. P.: CALIPSO mission: spaceborne lidar for observation of aerosols and clouds. In Lidar Remote Sensing for Industry and Environment Monitoring III, International Society for Optics and Photonics, 4893, 1–11, 2003.

Winker, D. M., Vaughan, M. A., Omar, A., Hu, Y., Powell, K. A., Liu, Z., Hunt, W. H., and Young, S. A.: Overview of the CALIPSO Mission and CALIOP Data Processing Algorithms, J. Atmos. Ocean. Tech., 26, 2310–2323, https://doi.org/10.1175/2009JTECHA1281.1, 2009.

Woods, C. and Caballero, R.: The role of moist intrusions in Winter Arctic warming and sea ice decline, J. Climate, 29, 4473–4485, https://doi.org/10.1175/JCLI-D-15-0773.1, 2016.

Xian, P., Reid, J. S., Turk, J. F., Hyer, E. J., and Westphal, D. L.: Impact of models versus satellite measured tropical precipitation on regional smoke optical thickness in an aerosol transport model, Geophys. Res. Lett., 36, L16805, https://doi.org/10.1029/2009GL038823, 2009.

Xian, P., Reid, J. S., Hyer, E. J., Sampson, C. R., Rubin, J. I., Ades, M., Asencio, N., Basart, S., Benedetti, A., Bhattacharjee, P. S., Brooks, M. E., Colarco, P. R., da Silva, A. M., Eck, T. F., Guth, J., Jorba, O., Kouznetsov, R., Kipling, Z., Sofiev, M., Perez Garcia-Pando, C., Pradhan, Y., Tanaka, T., Wang, J., Westphal, D. L., Yumimoto, K., and Zhang, J.: Current state of the global operational aerosol multi-model ensemble: An update from the International Cooperative for Aerosol Prediction (ICAP), Q. J. Roy. Meteor. Soc., 145, 176–209, https://doi.org/10.1002/qj.3497, 2019.

Xian, P., Klotzbach, P. J., Dunion, J. P., Janiga, M. A., Reid, J. S., Colarco, P. R., and Kipling, Z.: Revisiting the relationship between Atlantic dust and tropical cyclone activity using aerosol optical depth reanalyses: 2003–2018, Atmos. Chem. Phys., 20, 15357–15378, https://doi.org/10.5194/acp-20-15357-2020, 2020.

Xian, P., Zhang, J., Toth, T. D., Sorenson, B., Colarco, P. R., Kipling, Z., O'Neill, N. T., Hyer, E. J., Campell, J. R., Reid, J. S., and Ranjbar, K.: Arctic spring and summertime aerosol optical depth baseline from long-term observations and model reanalyses – Part 2: Statistics of extreme AOD events, and implications for the impact of regional biomass burning processes, Atmos. Chem. Phys., 22, 9949–9967, https://doi.org/10.5194/acp-22-9949-2022, 2022.

Xie, Y., Li, Z., Li, L., Wagener, R., Abboud, I., Li, K., Li, D., Zhang, Y., Chen, X., and Xu, H.: Aerosol optical, microphysical, chemical and radiative properties of high aerosol load cases over the Arctic based on AERONET measurements, Sci Rep.-UK, 8, 9376, https://doi.org/10.1038/s41598-018-27744-z, 2018.

Yang, Y., Wang, H., Smith, S. J., Easter, R. C., and Rasch, P. J.: Sulfate Aerosol in the Arctic: Source Attribution and Radiative Forcing, J. Geophys. Res.-Atmos., 123, 1899–1918, https://doi.org/10.1002/2017JD027298, 2018.

Zamora, L. M., Kahn, R. A., Cubison, M. J., Diskin, G. S., Jimenez, J. L., Kondo, Y., McFarquhar, G. M., Nenes, A., Thornhill, K. L., Wisthaler, A., Zelenyuk, A., and Ziemba, L. D.: Aircraft-measured indirect cloud effects from biomass burning smoke in the Arctic and subarctic, Atmos. Chem. Phys., 16, 715–738, https://doi.org/10.5194/acp-16-715-2016, 2016.

Zhang, J. and Reid, J. S.: A decadal regional and global trend analysis of the aerosol optical depth using a data-assimilation grade over-water MODIS and Level 2 MISR aerosol products, Atmos. Chem. Phys., 10, 10949–10963, https://doi.org/10.5194/acp-10-10949-2010, 2010.

Zhang, J., Reid, J. S., Alfaro-Contreras, R., and Xian, P.: Has China been exporting less particulate air pollution over the past decade?, Geophys. Res. Lett., 44, 2941–2948, https://doi.org/10.1002/2017GL072617, 2017.

Zhang, J., Spurr, R. J. D., Reid, J. S., Xian, P., Colarco, P. R., Campbell, J. R., Hyer, E. J., and Baker, N. L.: Development of an Ozone Monitoring Instrument (OMI) aerosol index (AI) data assimilation scheme for aerosol modeling over bright surfaces – a step toward direct radiance assimilation in the UV spectrum, Geosci. Model Dev., 14, 27–42, https://doi.org/10.5194/gmd-14-27-2021, 2021.

Zhang, J. and Reid, J. S.: MODIS Aerosol Product Analysis for Data Assimilation: Assessment of Level 2 Aerosol Optical Thickness Retrievals, J. Geophys. Res.-Atmos., 111, 22207, https://doi.org/10.1029/2005JD006898, 2006.

Zhang, J. L., Reid, J. S., Westphal, D. L., Baker, N. L., and Hyer, E. J.: A system for operational aerosol optical depth data assimilation over global oceans, J. Geophys. Res., 113, D10208, https://doi.org/10.1029/2007JD009065, 2008.

Zhang, Z., Wang, L., Xue, N., and Du, Z.: Spatiotemporal Analysis of Active Fires in the Arctic Region during 2001–2019 and a Fire Risk Assessment Model, Fire, 4, 57, https://doi.org/10.3390/fire4030057, 2021.

Zhao, C. and Garrett, T. J.: Effects of Arctic haze on surface cloud radiative forcing, Geophys. Res. Lett., 42, 557–564, https://doi.org/10.1002/2014GL062015, 2015.